Journal of Environmental Management 411 (2026) 130150

Contents lists available at ScienceDirect

Journal of Environmental Management

journal homepage: www.elsevier.com/locate/jenvman

Research article

Photocatalytic hydrogen driven (Pd-C\UV\H_2) advanced reduction process (ARP) for dechlorination and degradation of chlorotoluron in aqueous environment

Bakhtiar Ali Samejo [a], Ar. M. Fonlon [b], John M. Herbert [b], Marcin Łapiński [c], Jakub Karczewski [c], Sławomir Makowiec [d], Grzegorz Boczkaj [a,e,*]

[a] Department of Sanitary Engineering, Faculty of Civil and Environmental Engineering, Gdansk University of Technology, G. Narutowicza St. 11/12, Gdansk, Poland
[b] Department of Chemistry & Biochemistry, The Ohio State University, 151 W. Woodruff Ave., Columbus, OH, 43210, USA
[c] Faculty of Applied Physics and Mathematics, Institute of Nanotechnology and Materials Engineering, Gdańsk University of Technology, Narutowicza 11/12 Street, Gdańsk, 80-233, Poland
[d] Department of Organic Chemistry, Faculty of Chemistry, Gdansk University of Technology, G. Narutowicza St. 11/12, 80 – 233 Gdansk, Poland
[e] School of Civil, Environmental, and Architectural Engineering, College of Engineering, Korea University, 145 Anam-ro, Seongbuk-gu, Seoul, 02841, Republic of Korea

ARTICLE INFO

Keywords:
Photocatalysis
Hydrated electrons
Hydrogen radicals
Light-driven processes
Chemical agents

ABSTRACT

This paper present a novel investigation of the dechlorination and degradation of chlorotoluron (CHL) a persistent phenylurea herbicide type contaminant by the highly effective advanced reduction process (ARP), based on photocatalytic activation of hydrogen gas (H_2) by UV light and palladium on activated carbon (Pd-C) catalyst under aqueous conditions. Importantly, developed system is based on entirely new degradation mechanism which is much more effective comparing to typical UV-based or catalytic hydrogenation processes. The developed process is dedicated to wastewater treatment applications. This approach achieved >99.4% CHL reduction and >94.1% dechlorination at ambient temperature within 10 min. The degradation process followed a pseudo first order kinetics with k_{obs} of 0.1196 min^{-1}. Studies on degradation mechanism revealed contribution of generated hydrogen radicals ($H^{\bullet}$) and auxiliary role of hydrated electrons (e^{-}_{aq}). The reaction system was found to be very effective also in presence of inorganic anions. Performed studies proved stability of the performance over 5 cycles using same batch of catalyst. This part of the studies confirmed full applicability of the method for industrial practice. Operational costs of the treatment were estimated around 31.42$/$m^3$.

1. Introduction

The potential hazards to the environment and living beings that may result from the emission of Phenylurea herbicides (PUHs) residues are significant and cannot be overlooked due to the harmful side effects of overuse, high ecotoxicity risks (Marlatt and Martyniuk, 2017), and weak biodegradation (Gatidou et al., 2015; Federico et al., 2011). In order to ensure consumer health and improve fair international trade, the European Union has regulated maximum residue quantities of 0.5 μg/L for drinking water and 0.01–0.5 mg/kg for agricultural products. Importantly, there are up to 17 kinds of PUHs which have been prohibited (Badawi et al., 2009; Li et al., 2017). The harmful effects of chlortoluron (CHL) and its primary metabolites, including the carcinogenic azobenzene, on freshwater algae, aquatic invertebrates, and microorganisms have been demonstrated by ecotoxicological research (Lai et al., 2022). In addition, CHL has strong genotoxicity, persistency, and mobility in water. The extensive usage of these pesticides has created a serious trend that affects aquatic life and the ecosystem. Therefore, it is important to investigate the highly useful approach to remove these pesticides (Liu et al., 2024).

The degradation and transformation of PUH have been the subject of numerous researches to date. Adsorption (Tchikuala et al., 2017), microbial degradation (Tixier et al., 2000), chemical oxidation (Rosal et al., 2010; Lopez et al., 2001), biodegradation (Cullington and Walker, 1999; Wang et al., 2023), and advanced oxidation processes (AOPs) (Benitez et al., 2006, 2007a, 2007b) have all been shown to be

* Corresponding author. Department of Sanitary Engineering, Faculty of Civil and Environmental Engineering, Gdansk University of Technology, G. Narutowicza St. 11/12, Gdansk, Poland
E-mail addresses: grzegorz.boczkaj@pg.edu.pl, grzegorz_boczkaj@korea.ac.kr (G. Boczkaj).

https://doi.org/10.1016/j.jenvman.2026.130150
Received 31 March 2026; Received in revised form 11 May 2026; Accepted 4 June 2026
Available online 13 June 2026

significant in removal of PUH.

These methods do have some serious disadvantages, though, including poor kinetics, the production of hazardous byproducts, and high costs of treatment. On the other hand, Advanced Reduction Processes (ARPs), have received significant attention based on the generating highly active reductants and their effectiveness to reduce the persistent contaminants. These reductants possess powerful reducing electrode potential, i.e., e^-_{aq}, and $H^\bullet$ reduction potential are −2.9, and −2.3 V respectively, which make them effective for dehalogenation and further degradation of many refractory compounds (Park et al., 2009). Thus, ARPs is effective alternate to degrade impurities and yield non-harmful byproducts unlike AOPs and other approaches. Catalytic hydrogenation is widely used in organic chemistry and industrial processes to reduce unsaturated molecules into saturated compounds. Numerous pollutants, including phenols (Sun et al., 2014), NO_3^-, NO_2^-, BrO_3^-, and ClO_4^-, have been suggested to be treatable by catalytic hydrogenation (Prüsse and Vorlop, 2001; Yin et al., 2018; Chaplin et al., 2012). The catalytic reduction involves the use of a noble (Ru, Rh, Ir, Pd, Pt) and non-noble metal (Mn, Fe, Cu, Co, Ni) combination that is supported on a variety of materials, including carbon, alumina, hydrotalcites, and zeolites (Yuranova et al., 2012; Franch et al., 2012; Soares et al., 2011). The hydrogenation of bromates to bromide and the reduction of nitrates to nitrites are catalyzed by noble metal-based catalysts etc. Chen et al. (Chen et al., 2010) examined that Pd/Al_2O_3 exhibited high catalytic effectiveness and was utilized to hydrogenate bromate. Hao et al. proposed Pd nanoparticles (NPs) supported on a molecular organic framework (MOF) with hydrogen for phenol hydrogenation in the aqueous phase (Chen et al., 2018). Proto et al. (2015) reported that mayenite hydrides was used as a support for Pd to produce a selective and highly active catalyst for the benzaldehyde catalytic reduction in an H_2 environment (120 °C, 8 atm). In another study, Rhenium (Re)-Pd/C demonstrated a good catalytic activity at mild experimental conditions, enable the catalytic hydrogenation of perchlorate in water (Hurley and Shapley, 2007). Additionally, it has been observed that chlorinated organic pollutants in water may be effectively dechlorinated through catalytic hydrogenation(Chen et al., 2010).

The capacity of palladium (Pd) to activate water and generate atomic hydrogen radicals ($H^\bullet$) and electrons makes it a significant catalyst in catalytic reductive processes (Shao, 2011; Chaplin et al., 2012; Zhou et al., 2019). Additionally, under mild experimental conditions, Pd has a significant capability to facilitate C-Cl bond cleavage (Xu et al., 2013a, 2013b, 2016), which cause dechlorination from a variety of chloroaromatics (Sun et al., 2015; Li et al., 2012). It is suggested that Pd loading on catalysts with a large surface area will boost the formation of $H^\bullet$ due to spillover of H_2 (Li et al., 2016; sheng Wang et al., 2015; Tian et al., 2017). Typically, hydrogen adsorption on the surface of catalyst material improves the homolytic dissociation of H_2 gas into highly reactive $H^\bullet$ (Rehman et al., 2023).

Catalytic hydrogenation processes can be significantly improved and enhanced by photocatalytic reactions, which offer unique advantages for instance moderate reaction conditions and synergistic interactions between light and catalyst. Additionally, we examine the underlying mechanisms, the benefits of this hybrid approach, and how photocatalytic reactions enable photocatalytic hydrogenation process efficiency, could be improved via combining photocatalysis and hydrogenation (Chen et al., 2010; Heiden and Rauchfuss, 2007).

The complete performance of a photocatalytic system could be predicted and fine-tuned through modeling and optimizing the effect of each parameter. Response surface methodology (RSM) is a powerful tool for designing experiments that allow for the investigation of both individual and interactive effects of various variables simultaneously (Thind et al., 2018), unlike the conventional one which is slow and investigates one factor at a time (Lundstedt et al., 1998; Jiang et al., 2013). The most popular kind of RSM for modeling and optimizing the independent and interaction impacts of various factors in a catalytic system is central composite design (CCD) (Raizada et al., 2017; Mazhari et al., 2018; Bayuo et al., 2020).

In this work, the dechlorination and degradation of CHL in novel UV/Pd-C/H_2-ARP approach was studied. RSM was used to analyze the collective impacts of three relevant operating parameters on CHL degradation efficiency, including H_2 flow, Pd-C concentration, and solution pH and the optimum conditions were predicted, followed by experimental confirmation. The radical quenching studies verified the presence of the main reaction active species in the process. Additionally, this study shown the first reported application of a ARP-based approach utilizing UV/Pd-C/H_2 system for the degradation of CHL. Likewise, in comparison to the UV/Pd-C/H_2 technique, the degrading efficiency of CHL by less complex treatment systems, including UV/Pd-C/S/H_2, UV/S/H_2, UV/Pd-C, UV/S, UV/H_2, and sole processes were also investigated. Based on HPLC with UV-VIS detector and GC-MS degradation intermediates were identified, and possible CHL degradation pathways in the UV/Pd-C/H_2 process were proposed. Importantly, the developed system offers new degradation mechanism that can gain usefulness also for degradation of other persistent organic pollutants. The energy usage of this system was also assessed. Furthermore, the cyclability and stability of Pd-C were assessed in five successive experimental cycles regarding their practical applications.

2. Materials and methods

2.1. Materials

Details of the chemicals used in the study of CHL degradation are given in Text S1, and without further purification all the materials were utilized.

2.2. Experimental procedures

2.2.1. Preparation of chlorotoluron solution

A 20 mg/L CHL solution was prepared in 700 mL of DI water. CHL quantity was weighed on an analytical weight balance (model: AS.310. R2, RADWAG, Poland) with an accuracy of 0.1 mg. The CHL solution was obtained by continuous stirring the liquid in a closed container using a magnetic stirrer (model: 06 MSH PRO T, Chemland, Stargard, Poland).

2.2.2. Degradation experiments

A 1 L cylindrical photo-reactor (Lelesil Innovative System, India) with an active volume of 700 mL was utilized for all of the experiments. The H_2 gas was supplied by the hydrogen generator $PGXH_2$ 500 (PerkinElmer, USA) model. The H_2 gas (purity >99.995%) flowrate into the reactor was regulated by a gas rotameter (Krohne Duisburq, Germany) from 1 to 4 L/h range. H_2 gas was injected into the liquid using a frit providing dispersion of H_2 into small bubbles. A schematic diagram of the photo-reactor is added in Fig. 1. In case of experiments performed with addition of sodium sulfite before starting the analysis, it was added to the model solution to remove soluble oxygen. The photo-reactor had inner diameter of 100 mm and 270 mm height. The UV light was placed in the center of the reactor within a quartz tube with a 30 mm outer diameter. A magnetic stirrer was utilized to constantly stir the solution. To irradiate light on the CHL samples, a UV lamp (Mercury, 450 W lamp) was used. The lamp had a wavelength of around 254 nm. Throughout the experiments, cooling water was continuously pumped across the UV reactor to keep the system at the desired temperature (20 °C).

A model solution of CHL with initial concentration of 20 mg/L was placed in the reactor. Prior to UV irradiation, the Pd-C catalyst was added into the model solution and equilibrated for 30 min (time selected during preliminary studies). Samples were collected both before addition of Pd-C catalyst and after 30 min of equilibration. On this basis the contribution of adsorption phenomenon on the removal effectiveness was evaluated. The dissolved oxygen content of model solution was

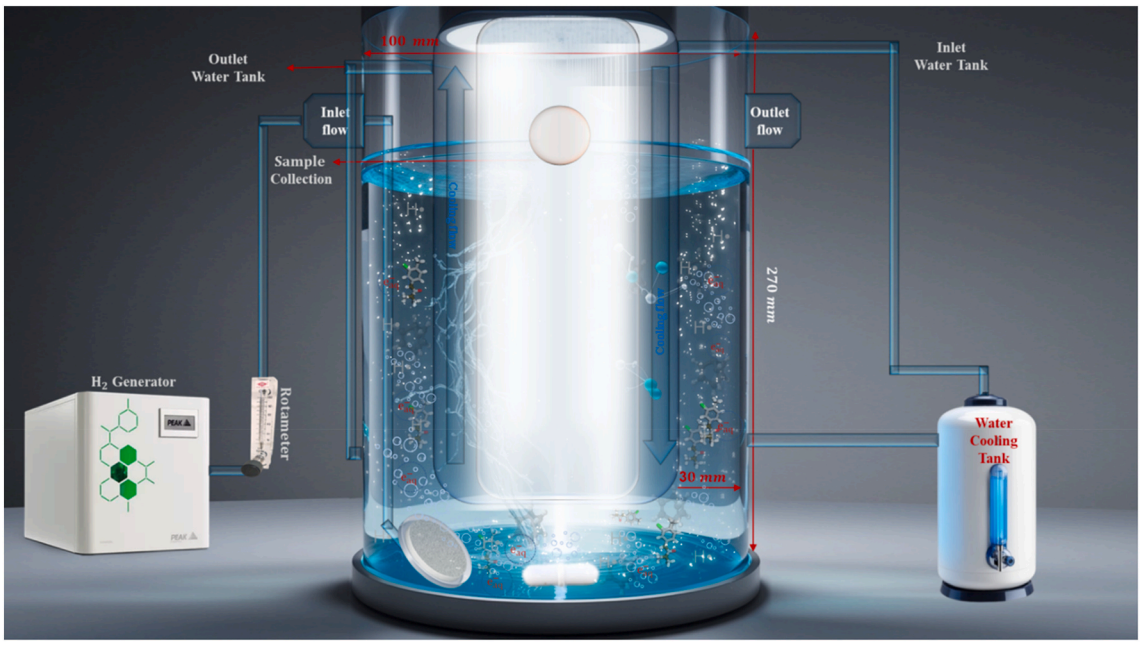

Fig. 1. Schematic scheme of UV reactor, connected with H_2 generator and water cooling system for UV reactor (a photography of the experimental setup is presented on Fig. S1). A rotameter is connected to H_2 generator to regulate the flow and stirrer was used for proper mixing.

measured before and after the experiment by an electric meter (CCO-401, Elmetron) equipped with an oxygen sensor (COG-1, Elmetron).

At the proper time intervals, samples were collected from a dedicated valve in the reactor for HPLC analysis. For comparison, control experiments were conducted without UV exposure to account for natural degradation processes. Also, effect of inorganic anions and humic acid was investigated. The scavenging test were carried out by iron (III) cations (Fe^{3+}), NO_3^- and NO_2^- to determine the reactive reductive radicals involved in the degradation process.

2.2.3. Characterization of Pd catalyst (SEM, EDS, XRD, XPS)

Different characterization techniques were used to examine the Pd catalyst properties, scanning electron microscopy (SEM, FEI Quanta 250) were performed to examine the morphology and crystalline phases of Pd-C were examined via X-ray diffraction (XRD, PANalytical X′ Pert PRO X-ray diffractometer). Chemical composition and valency were investigated by X-ray photoelectron spectroscopy (XPS, Omiocron NanoTechnology), see text S2 for details.

2.2.4. Ultra-high performance liquid chromatography (UHPLC) analysis

Separation was carried out in ultra-high performance liquid chromatography (UHPLC, Nexera XS system (USA)), see text S3 for separation details.

2.2.5. Control of Pd leaching into water – ICP-OES analysis

The Pd concentration in post-processed model solutions was determined by inductively coupled plasma optical emission spectrometry (ICP-OES), Text S4 shows the detailed measurement conditions of leached Pd catalyst before and after degradation processes.

2.2.6. Identification of degradation by-products – gas chromatography coupled with mass spectrometry (GC-MS)

A gas chromatograph (model GC-2010 Plus, Shimadzu, Japan) with mass spectrometer (GC-MS, model QP2010SE, Shimadzu, Japan) was utilized to run the chromatographic examination of degradation intermediates. Conditions of the analysis are given in Text S5.

2.2.7. Anion identification/quantification by ion chromatography

Chloride ions concentration was determined by ion chromatography (Dionex Aquion, Thermo Scientific, USA), see text S6 for identification and quantification details.

2.2.8. Performance indices

The degradation of CHL was calculated by Eq. (1).

$$\textit{Degradation effectiveness} = \frac{C_o - C_t}{C_o} \times 100\% \quad \text{Eq. (1)}$$

Where C_o, C_t were concentration of CHL (mg/L) at the start and time of reaction.

The dechlorination effectiveness was determined via (Eq. (2)):

$$\textit{Dechlorination effectiveness}\ (\%) = \left(\frac{212.67 \times \{Cl_t^- - Cl_0^-\}}{35.5 \times 1 \times C_o}\right) \times 100\% \quad \text{Eq. (2)}$$

where Cl_0^- and Cl_t^- was the concentration of chloride ions (mg/L), C_o was the initial concentration of CHL (mg/L). Additionally fixed constants of 212.67, 35.5 and 1 are the molecular masses of CHL, Cl^- and one chloride ion in CHL molecule respectively (Moussavi and Rezaei, 2017).

2.3. Response surface methodology

In this study, the response surface methodology (RSM) based on central composite design (CCD) was used. A statistical technique named as RSM may be utilized to model, evaluate how multivariable alter response values, and enhance operating parameters (Bezerra et al., 2008; Liu et al., 2022a). CCD of RSM was developed and optimized the CHL reduction experiment. A three-variable H_2 flow (X_1), Pd-C catalyst dosage (X_2) and pH (X_3) and five-levels ($-\alpha$, -1, 0, $+1$, $+\alpha$) of CCD with total of 20 number experiments were run in an irregular order to diminish systematic errors provided in Table 1S. The H_2 gas flow ranged from 1 to 4 L/h, Pd-C catalyst dosage was selected at mass ratios from 1 to 4 in respect to CHL pollutant (20 mg/L model solution) abbreviated as Pd-C:CHL = 1:2, 2:2, 3:2 and 4:2. While, pH ranged from 2 to 12. CCD design and subsequent evaluation of data were performed by the Design Expert (13.0.5.0) software.

The details of empirical second-order polynomial equation (Eq. (1S)) (Song et al., 2020) used for CCD analysis is shown in Text S7.

2.4. Computational analysis for CHL

The "condensed" Fukui function (Pucci and Angilella, 2022; Fuentealba et al., 2000) maps the continuously valued Fukui function onto atomic indices that are used as parameters to indicate reactive sites in molecules based on a change in the electronic density upon addition or removal of electrons (Elakiya et al., 2017; Chu et al., 2025). For radical attack, the Fukui function $f_k^0(\mathbf{r})$ is mapped onto atomic indices as (Eq, 3)

$$f_k^0 = \frac{1}{2}\left[q_k(N+1) - q_k(N-1)\right] \quad \text{Eq. (3)}$$

where q_k $(N+1)$ and q_k $(N-1)$ are the electron populations for the molecular anion (with $N+1$ electrons) and the cation, respectively. Atoms with larger indices are associated with higher reactivity toward radical

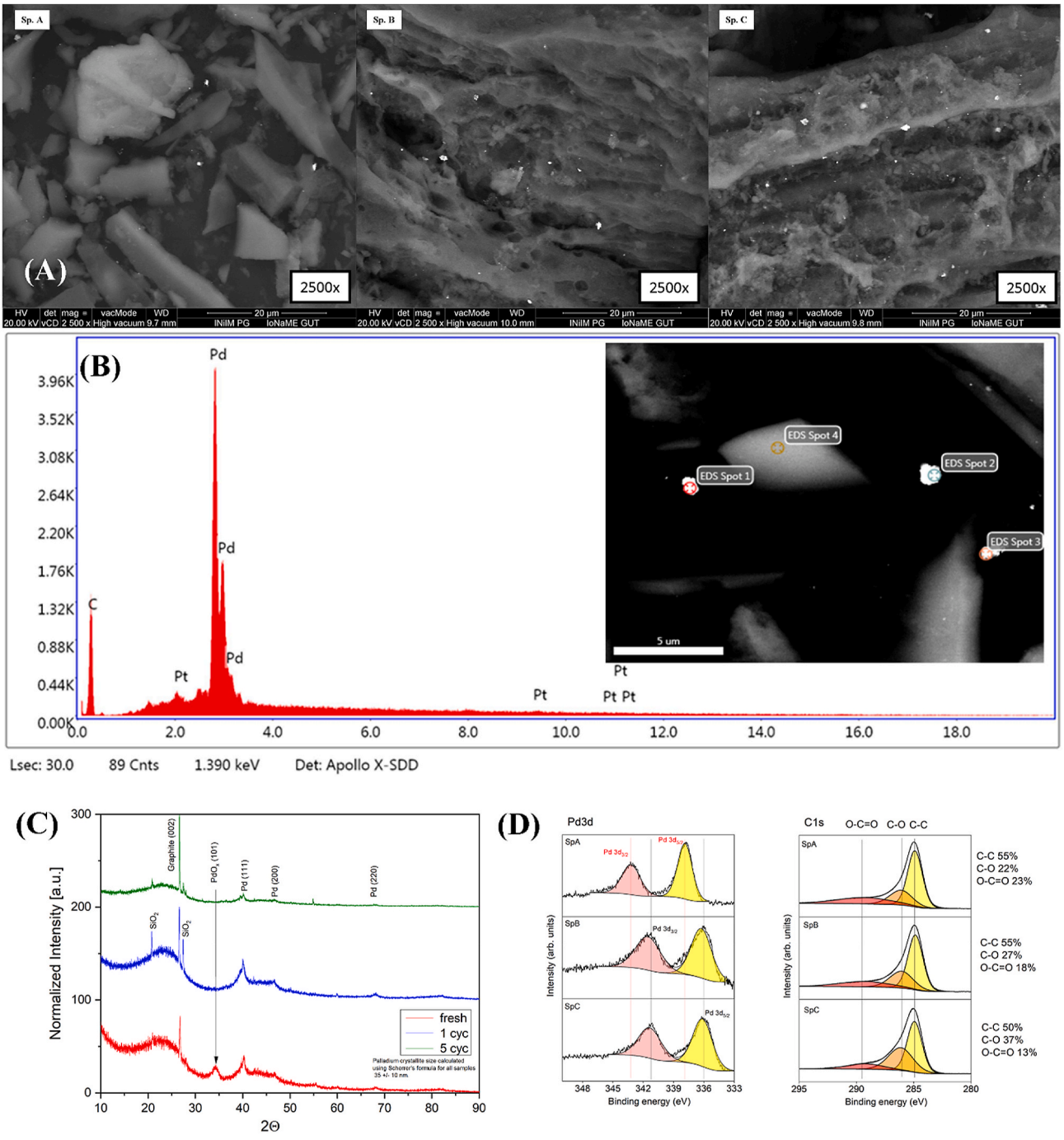

Fig. 2. (A) SEM images of SpA, SpB and SpC corresponding to fresh, 1st and 5th cycle Pd-C catalyst at 20 μm scale (2500× resolution) shows the overall surface morphology and (b) EDS spectrum of fresh Pd-C at spot 2 gives the mass content of Pd, different spots are given in the inset image which provide the mass content of Pd on AC support. (c) XRD patterns of Pd-C catalyst in the fresh, and after catalytic cycles. Diffraction peaks observed at approximately 40.1°, 46.7°, and 68.1° (2θ) correspond to the (111), (200), and (220) planes of Pd. (d) High resolution XPS spectra of (i) Pd 3 d and (ii) C1s spectra for Pd/AC catalyst. Pd 3 d spectra of three different samples, SpA, SpB and SpC corresponding to fresh, 1st and 5th cycle, respectively. The Pd 3 d spectra demonstrate a shift from Pd^{4+} (338 eV/343 eV) in the fresh catalyst to Pd^{2+} (336 eV/341 eV) after reduction. The C1s spectra confirm the presence of various surface functionalities, including C–C, C–O, and O–C=O groups on the AC support.

attack (Table 2S) (Elakiya et al., 2017; Chu et al., 2025). In the present work, we use atomic charges computed from natural population analysis (Reed et al., 1985). All calculations were performed at the ωB97X-D/def2-SV(P) level of theory (Weigend and Ahlrichs, 2005; Chai and Head-Gordon, 2008), using Q-Chem v. 6.3 (Epifanovsky et al., 2021).

3. Results and discussion

3.1. Characteristics of Pd-C before and after analysis

Imaging of the Pd-C catalyst was conducted using a backscattered electron (BSE) detector, enabling the identification of objects composed of elements with varying atomic numbers. Scanning electron microscopy (SEM) images distinctly reveal a homogeneous distribution of particles characterized by significant contrast, indicating that these are nanoparticles (NPs) made from elements with considerably higher atomic numbers than carbon. Energy-dispersive spectroscopy (EDS) analysis of individual particles demonstrates that the majority of them contain palladium; (however, a fraction also shows some presence of platinum, which probably come from impurity of reagents used in large scale synthesis, as the used catalyst is commercially available). The SEM image of Pd-C (Fig. 2a) clearly indicated that Pd NPs covered the surface of AC. Catalyst surface of 1st and 5th cycles were found to possess a rugged, large flakes, undefined morphology, on which Pd NPs were loaded and there was no major difference obtained compared to fresh Pd-C. The Pd NPs remained uniformly dispersed, and their size was consistent across all samples. This suggested strong interaction between Pd and the AC support, contributing to the catalyst's excellent structural stability and reusability over multiple cycles. EDS images confirmed homogeneous dispersion of Pd nanoparticles in the fresh catalyst, while very mild aggregation was observed after repeated catalytic cycles (Fig. 2b).

This supported the conclusion that the catalyst maintained reasonable structural integrity and metal dispersion upon reuse (Fig. S2 (EDS of 2 samples of fresh and 1st cycle)). Also, in the fresh catalyst small traces of Pt were observed, suggesting either trace contamination or co-deposition in the synthesis process. The XRD patterns of the Pd-C fresh and after cycles samples are shown in Fig. 2c. The average palladium crystallite size was calculated using Scherrer's formula for all samples around 35 ± 10 nm.

XRD analysis of the Pd-C catalyst obtained diffraction peaks at 2θ of 34.4° is assigned to the (101) facet of PdO (Cho et al., 2018; Hu et al., 2017). A verification of the occurrence of Pd was confirmed by the observation of peaks at 2 θ of 40.1°, 46.7°, and a small peak at 68.1°, these peaks relate to the (111), (200), and (220) planes of Pd, respectively (Lan et al., 2016; Zhao et al., 2020). The intensities of the corresponding PdO XRD peak from the fresh Pd-C catalyst showed a significant decrease, compared to that of the 1st and 5th cycle Pd-C catalyst, confirming the complete reduction of PdO (Pd^{4+}) content to Pd^{2+}/Pd^{0}. Furthermore, a broad peak was observed in all samples at 2θ, which was ~25°. This peak was formed via the (002) diffraction lines of graphite microcrystals in the carbon (Xu et al., 2019; Lan et al., 2016; Crawford et al., 2021).

The chemical composition and valency of Pd NPs supported on AC were observed through XPS investigation both before and after (after the 1st and 5th cycles) the dechlorination/degradation of CHL. The high-resolution Pd 3 d spectra consist of two well-defined peaks forming a characteristic doublet. Based on the peak fitting analysis presented in Fig. 2d, the fresh Pd $3d_{5/2}$ and $3d_{3/2}$ peaks for the Pd-on-carbon catalyst appear at approximately 337.5 eV and 343.4 eV, respectively, corresponding to Pd^{4+} species (Han et al., 2017; Lv et al., 2019; Li et al., 2025), suggesting that palladium initially existed in a highly oxidized form before the reaction (Meher and Rana, 2019; Crawford et al., 2021; Xie et al., 2023). A significant alteration in the Pd 3 d peaks was observed after exposure to H_2 gas during the reduction process. The post-reaction spectra (after the 1st and 5th cycles) exhibited peaks at approximately 336.0 eV and 341.3 eV, indicative of Pd^{2+} species, typically attributed to PdO. The transition from Pd^{4+} to Pd^{2+} indicates that the palladium surface underwent in-situ reduction in the presence of H_2, consistent with its expected catalytic role in hydrogenation or reduction reactions. According to Karatok et al. (2020), oxidized Pd were easily reduced at 300 K, and H_2 dissociated on oxidized Pd surfaces. This corelated our observation that the H_2 gas in the ARP system induced a progressive in-situ reduction of Pd^{4+} to Pd^{2+} under ambient reaction conditions. This was confirmed by the XPS shift from approximately 338 eV in the fresh catalyst to approx. 336 eV (Karatok et al., 2020). Additionally, fresh catalyst Pd^{4+}, coordinated via PdO_x bond in an octahedral like structure (Koga, 2020; Kibis et al., 2012), it has been reported that Pd^{4+} participate in catalytic cycle with H_2 through the Pd^{4+} to Pd^{2+} mechanism (Koga, 2020), under the air/H_2 gas phase conditions. Liu et al. (2022b) described photocatalytic CO_2 reduction in aqueous medium by employing Pd NPs on C_3N_4, and the active sites of Pd NPs were responsible to generate H* atoms. Whereas, transiently produced Pd^{0} enabled H_2 dissociation, which induced C-Cl bond hydrogenolysis in CHL (Wilde et al., 2008; Chaplin et al., 2012;Conrad et al., 1974; Hoke et al., 1992). Moreover, in all three spectra, the absence of dominant peaks around 335 eV—characteristic of metallic Pd^{0}—suggests that complete reduction to the metallic state either did not occur or was not predominant under the given reaction conditions (Kibis et al., 2012; Gómez-Quero et al., 2008). These findings support the notion that the Pd-C catalyst enhanced CHL reduction, with palladium acting as an active redox mediator. The XPS data thus provide strong evidence of catalytic involvement, showing that the surface chemistry of Pd changed in response to the reducing environment and likely facilitated CHL dechlorination/degradation (Crawford et al., 2021; Li et al., 2025). Furthermore, the C 1s spectrum exhibited typical peaks at ~284.6 eV (C–C), ~286.2 eV (C–O), and ~288.5 eV (O–C=O), reflecting the functional groups present on the activated carbon surface (Fujimoto et al., 2016; Suyana et al., 2016; Chen et al., 2020). These groups may contribute to the anchoring and dispersion of Pd NPs.

3.2. The role of UV, S, Pd-C and H_2 for the generation of radicals

Degradation effectiveness of various processes from sole experiments to complex (UV/S, UV/H_2, UV/Pd-C, etc.) were examined. Sole sulfite (S) was not effective to degrade CHL. While, the stability and limited reactivity of H_2 make it ineffective in degrading CHL.

Sole UV light can directly break chemical bonds in organic molecules, leading to degradation or the formation of reactive intermediates. In case of CHL, UV light could initiate bond cleavage, in the C-Cl bond or aromatic ring. UV sole can also produce hydroxyl radicals ($OH^{\bullet}$), hence to confirm the effect of $OH^{\bullet}$, scavenging test was performed in presence of methanol (MeOH). On the other hand, UV can be used to activate reductants to produce radical species.

During UV irradiation, S, H_2 gas on Pd-C surface (Zhao et al., 2022; Li et al., 2015) and water molecules can be photo-excited to produce $SO_3^{\bullet -}$, $H^{\bullet}$, e^-_{aq}, and $OH^{\bullet}$ (Eqs. (4)–(8)) (Wu et al., 2021; Chen et al., 2022).

$$SO_3^{2-} + h\nu \rightarrow SO_3^{\cdot -} + e^-_{aq} \quad \text{Eq. (4)}$$

$$H_2 \xrightarrow{PdC+h\nu} H^{\cdot} \quad \text{Eq. (5)}$$

$$H_2O + UV \rightarrow HO^{\cdot} + H^+ + e^-_{aq} \quad \text{Eq. (6)}$$

$$H_2O + UV \rightarrow HO^{\cdot} + H^{\cdot} \quad \text{Eq. (7)}$$

$$H^{\cdot} + H_2O \rightarrow e^-_{aq} + H^+ \quad \text{Eq. (8)}$$

Sole UV could not completely degrade the CHL pollutant which was around 75.8% in 1 h. As sole UV process did not provide sufficient

effectiveness, in next stage direct activation of reductants by UV was studied. UV/S and UV/H_2 processes demonstrated good degradation compared to sole UV. The combination of UV light with S and H_2 enhanced reduction processes. The generated reducing radicals contributed to break bonds in the CHL. UV/S procedure enhanced the degradation by producing different reductants (Eq. (4)). While, in the UV/H_2 process, the homolytic photodissociation did not occur effectively with UV-C light, though to some extent high power UV reactor (450 W) might manage to generate the $H^{\bullet}$ radicals (Qerimi et al., 2020; Hernandez et al., 2024) and observed slightly higher degradation efficiency than sole UV (Eqs. (6)–(8)). However, the efficiency of UV/S process was higher than UV/H_2, this could be owing to large number of different reductants produced in the former process, and still hard to activate enough $H^{\bullet}$ radicals via the UV source with 254 nm, also the less water solubility of H_2 (Wiebe and Gaddy, 1934; Chabab et al., 2024) caused less number of $H^{\bullet}$ radicals. Additionally, UV/Pd-C photocatalytic approach was used to degrade CHL, the quantum efficiency of Pd-C excitation was low, these small number of excited electrons of Pd-C catalyst can be transported to adsorbed electron-deficient pollutant thus slight increase in degradation effectiveness was seen (Eq. (5)) (Waddell et al., 2023; Abdelhameed et al., 2024).

Finally, the most complex processes; S and H_2-based photocatalytic hydrogenation (UV/S/Pd-C/H_2) process and (UV/Pd-C/H_2) process respectively were examined. UV/S/Pd-C/H_2 and UV/Pd-C/H_2 processes showed highest dechlorination/degradation effectiveness of CHL compared to other approaches. These processes produced large number of reactive reductants. While, Pd-C is a widely used heterogeneous catalyst in hydrogenation and reduction reactions by adsorbing H_2 and dissociating it into atomic hydrogen. Owing to metallic nature of Pd, there are free electrons close to the Fermi level, allowing for continuous electron flow. This property is supported by theoretical and electrochemical investigations (Gonçalves et al., 2023; Wei et al., 2018; Phan et al., 2006).

The partially occupied d-orbitals can accept the electron of H_2, meanwhile the d-electrons can donate to the δ^* antibonding orbital of H_2, this is why the H–H bonds are cleaved followed by formation of M–H species. Effective increase of the electron density of metal sites enhances hydrogenation performance of the photocatalytic process (Guo et al., 2022).

3.3. Degradation and dechlorination of CHL by ARP

3.3.1. Comparison of effectiveness and degradation kinetics of ARP systems

The degradation effectiveness of CHL by UV/Pd-C/S/H_2, UV/Pd-C/H_2, UV/S/H_2, UV/Pd-C, UV/S, UV/H_2 and for comparison sole experiments were also examined. These degradation processes of PUH followed the pseudo-first order kinetics. Using pseudo first-order kinetics, the degradation rate of the pollutants could be calculated by Eq. (9).

$$-\frac{\ln[CHL]_t}{\ln[CHL]_s} = k_{obs} \times t \qquad \text{Eq. (9)}$$

where $[CHL]_t$ and $[CHL]_o$ mean concentrations of PUH (mg/L) at t = t and t = 0 (s), respectively, and k_{obs} represents the pseudo first-order rate constant (min^{-1}).

The k_{obs} plot of CHL degradation after 15 min by different approaches are shown in Fig. 3a, which obtained a histogram of k_{obs}. In this study, experiments were carried out under parameters pre-selected based on preliminary experiments, i.e. Pd-C:CHL = 2:2 mass ratio, $r_{red.}$ = 10, H_2 = 2 L/h, CHL = 20 mg/L and pH = 7, which later served as reference for the subsequent optimization. The degradation of CHL by different approaches within 60 min followed the order of UV/Pd-C/H_2 (99.7%) > Pd-C/H_2 (97.5%) > UV/S/Pd-C/H_2 (96.2%) > UV/S (93.1%) > UV/S/H_2 (91.2%) > UV/H_2 (87.0%) > UV/Pd-C (85.8%) > UV lone (75.8%). The orders of dechlorination efficiencies were ranked as UV/Pd-C/H_2 (88.5%) > UV/Pd-C (75.1%) > UV/S/H_2 (55.5%) > UV/S (54.3%) > UV/S/Pd-C/H_2 (52.2%) > UV/H_2 (42.5%) > UV lone (28.4%) (dechlorination of some of the effective processes in Fig. S3a). This is supported with the facts that the sole use of Pd-C and SO_3^{2-} cannot generate enough radicals.

In addition, under common conditions at 20 °C, water solution contain ~1.3×10^{-3} mol/L (41.6 mg/L) of dissolved oxygen (Xing et al., 2014). Higher oxygen quantity demand more reducing agent to remove oxygen. Thus, numerous deoxygenation processes such as sonication, inert gas purging, and high heating should be considered (Cako et al., 2022; Cichocki et al., 2024).

In this study, before starting the experiment the oxygen content in the CHL model solution was higher than 70% (6.37 mg/L) of oxygen solubility (in respect to saturation value) which was deoxygenated by adding Na_2SO_3 salt and in another experiment H_2 flow was utilized that simultaneously performed as reductant and purging gas, however, almost similar degradation was achieved in the presence and absence of oxygen in the UV/Pd-C/H_2 process and after complete CHL degradation oxygen saturation content was measured <20% (1.82 mg/L) using an oxygen selective electrode. Thus, oxygen presence did not show significant changes in the degradation of CHL at similar parameters.

Moreover, it was observed that the UV/S/Pd-C/H_2 showed lower degradation (k_{obs} 0.0546 min^{-1}) than UV/Pd-C/H_2 (k_{obs} 0.1196 min^{-1}) process. Although, SO_3^{2-} is a strong reductant (E_0: $SO_3^{\bullet -}$/SO_3^{2-}) = 0.73 ± 0.01 V vs NHE.) (Das et al., 1999), it exhibited the weak reductive ability toward CHL and had less impact on CHL degradation

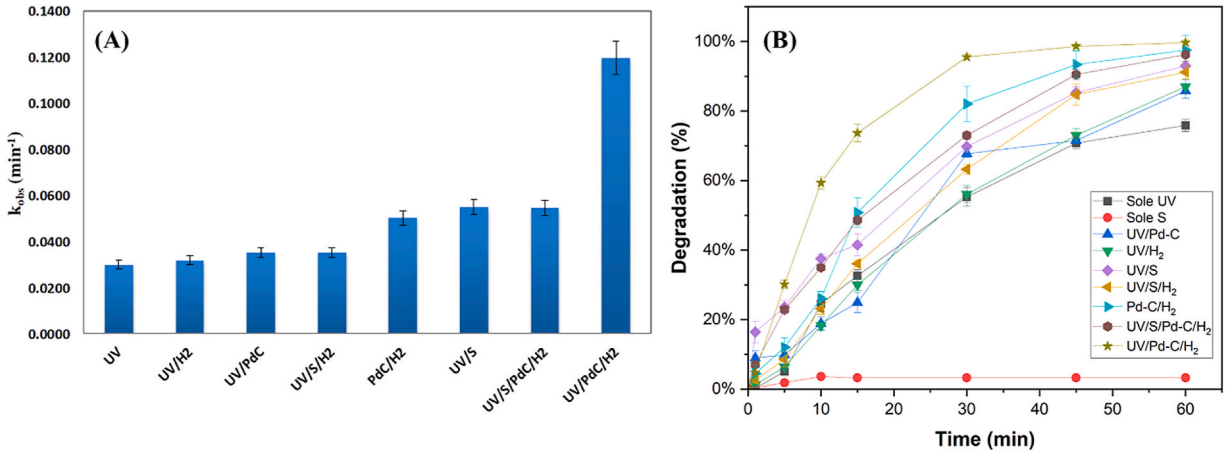

Fig. 3. (A) Pseudo-first-order kinetics plot of CHL by various methods at conditions of Pd-C:CHL = 2:2, r_{red} = 10, H_2 = 2 L/h, CHL = 20 mg/L and pH = 7, and (b) degradation and dechlorination of CHL by various methods at conditions of Pd-C:CHL = 2:2, $r_{red.}$ = 10, H_2 = 2 L/h, CHL = 20 mg/L and pH = 7.

compared to of $H^{\bullet}$ radicals and hydrated electron. Thus, it can be suggested that the SO_3^{2-} scavenged other reductants in the reaction. On the other hand, sulfur containing compounds poison the Pd-C catalyst surface in many hydrogenation processes (V Lowry and Reinhard, 2000; Zhang et al., 2013). In addition, effect of catalyst poisoning was investigated at different pH range (Fig. S3b) and SO_3^{2-} concentrations (Fig. S3c) to observe the degradation effectiveness. It was observed that under alkaline conditions complete degradation was observed, while pH 4 and 7 obtained degradation was around 69.4 and 83.5% in 1 h, respectively. This performance could be attributed to the diminished production of radicals due to HSO_3^- dominance at acidic environment and poisoned Pd surface, which inhibited H_2 activation. At pH 10, compared to HSO_3^-, effective photoionization of SO_3^{2-} occurred, as SO_3^{2-} possess high quantum yield of e_{aq}^- production (Samejo et al., 2025), thus, at alkaline condition, partial conversion of SO_3^{2-} improved degradation. Therefore, as pH increased, a balanced performance between catalyst poisoning and SO_3^{2-} based radical generation observed (Samejo et al., 2025; Navon et al., 2012). Moreover, effect of SO_3^{2-} concentration at $r_{red} = 5$, shown that the Pd catalyst poisoning effect was lower than $r_{red} = 10$ and 20. At $r_{red} = 10$, stronger deactivation effect was observed. Nonetheless, $r_{red} = 20$ obtained slightly high degradation compared to $r_{red} = 10$, this suggested that, beside the poisoning of Pd catalyst high SO_3^{2-} concentration favored the generation of more radicals (Navon et al., 2012; Yuan et al., 2013).

While, UV/Pd-C/H_2 significantly increased CHL degradation and the generation of e_{aq}^- and $H^{\bullet}$ radicals from the UV/Pd-C/H_2 photolysis of H_2O (Eqs. (6)–(8)) (Gu et al., 2017). Also, CHL degradation in UV/Pd-C/H_2 was much faster due to more reactive radicals formation than other approaches (Fig. 3b).

In addition, UV/S/H_2 process exhibited degradation/dechlorination up to 91.2 and 71.9% respectively, and Pd-C/H_2 revealed 87.3 % degradation of CHL with 66.1% dechlorination owing to less intensive formation of radicals. UV/H_2 showed 84.9% degradation and 62.4% dechlorination. UV/S possessed good degradation (90.1%), where $SO_3^{\bullet-}$ radicals (Fedorov et al., 2025; Samejo et al., 2025) were actively participated. In UV/Pd-C enough hydrogen radicals were generated and exhibited good removal. Additionally, UV sole process exhibited good degradation rate of 0.0299 min^{-1}. Moreover, UV/Pd-C/H_2 process was compared against the UV/SO_3^{2-} (UV/S) and UV/dithionite (UV/DTN) approaches under the same pH conditions and selected molar ratio was $r_{red} = 10$. UV/Pd-C/H_2 process acquired >99% degradation within 1 h, whereas UV/S and UV/DTN obtained 49.2% and 36.5% in 1 h, respectively (Fig. S3d), thus UV/Pd-C/H_2 photocatalytic system highlighted the highest performance.

In summary, these outcomes suggested that UV/Pd-C/H_2 could concurrently attain superior dechlorination and degradation of CHL through photocatalysis-driven radical reactions. While processes where sulfite was utilized, the efficiency was decreased, due to the scavenging reaction of $SO_3^{\bullet-}$ with e_{aq}^- and $H^{\bullet}$ radicals (Eqs. (10)–(12)) and SO_3^{2-} can adsorb on the Pd-C catalytic surface area, which diminish the availability of active sites for H_2 dissociation or electron transfer.

$$SO_3^{2-} + h\nu \rightarrow SO_3^{\cdot-} + e_{aq}^- \quad (10)$$

$$SO_3^{\cdot-} + e_{aq}^- \rightarrow SO_3^{2-} \quad (11)$$

$$H^{\cdot} + SO_3^{\cdot-} \rightarrow HSO_3^- \quad (12)$$

Recent research degraded CHL to undesirable byproducts via UV/PS ($HO^{\bullet}$ and $SO_4^{\bullet-}$) (Lai et al., 2022). Since these intermediates are hardly reduced to small molecules like CO_2, the hydroxylation and successive oxidation of aromatic compounds and alkyl groups led to a limited mineralization of the contaminant by-products.

3.3.2. CCD model optimization of photocatalytic performance

The CCD procedure was utilized to optimize the photocatalytic degradation of CHL by optimizing three independent variables (Mazhari et al., 2018). The results of twenty runs of the CHL reduction experiment are shown in Table 3S, along with the real and predicted values of how well CHL degraded in 30 min based on the changes between the three factors. The obtained linear model with three independent variables are shown by the following Eq. (13) of Y (predicted response, i.e. CHL degradation %):

$$Y = +85.642859379077 + 1.31418X_{1(A)} + 2.94214X_{2(B)} - 0.051251X_{3(C)} \quad \text{Eq. (13)}$$

ANOVA was employed to examine the significance and reliability of model (see Table 4S).

Meanwhile, the high p-value (>0.05) indicates that the lack of fit (1.24) is not statistically significant. This is a desirable outcome, as it suggests that the model fits the data well and does not miss any critical patterns. Moreover, the model was reliable as the coefficient of determination R^2 of 0.9020 and adjusted R^2 (0.8836) showed close values (Mazhari et al., 2018). The validity of model was verified by the high agreement between experimental and estimated values (Fig. S4). The R^2 value of 0.9020 stated that the independent variables and their interaction in the model impacted greatly on CHL degradation efficiency. The p-value of interactions in Table 4S was less than <0.0001, which suggested that the interactions between the parameters were significant.

The model reveals a good fit for the data, explaining most of the variation in the response variable (75.22 out of 83.39). The F-test of model is significant, suggesting that the predictors collectively contribute to predicting the response variable.

Moreover, the three-dimensional (3D) response surface and two-dimensional (2D) contour plots of the interaction between variables are shown in Fig. 4. Contour plots displayed significant variable interaction, as increasing Pd-C amount extent which provides more radical formation and the interaction with pollutant hence enhances the CHL photocatalytic degradation efficiency. While, the third variable pH was statistically significant. This factor suggested that pH effect in CHL degradation was enhanced in acidic medium (Liu et al., 2022a).

The numerical optimization function of the CCD determined the optimal conditions for maximum CHL degradation effectiveness was observed >99% within 10 min at a H_2 flow rate of 4 L/h, a Pd-C:CHL ratio of 4:2, and an acidic pH (4), as shown in table 3S. Experimental validation at these conditions closely matched the predicted values, confirming the model's reliability.

3.3.3. Discussion of optimization conditions

The optimal values of the different factors were studied for the CHL degradation via photocatalytic hydrogenation based ARP approach.

3.3.3.1. Effect of pH. Typically, wastewater pH has a critical impact on degradation process effectiveness. Therefore, CHL reduction was examined by the effect of pH. The study was conducted from 2 to 12 pH scale, with an optimized parameters of UV/Pd-C/H_2 process at CHL 20 mg/L, H_2 gas to 2 L/h, and Pd-C:CHL = 2:1 (or 4:2) mass ratio.

CHL reduction was affected after altering the pH, i.e., $H^{\bullet}$ and e_{aq}^- conversion occur. e_{aq}^- dominated the reduction procedure at pH 7 where both reductants contributed, while at acidic pH, e_{aq}^- is rapidly quenched by H^+ to produce $H^{\bullet}$, whereas $H^{\bullet}$ reacts with OH^- to form e_{aq}^- at pH > 8.7 (Eqs. (14) and (15)). On the other hand, pH increase cause decrease in quenching rate (e_{aq}^- by H^+) by one order of magnitude (Samejo et al., 2025). Therefore, production of $H^{\bullet}$ increases which seemed favorable for reduction.

$$H^+ + e_{aq}^- \rightarrow H^{\cdot} \quad (k = 2.3 \times 10^{10} M^{-} s^{-}) \quad \text{Eq. (14)}$$

$$HO^- + H^{\cdot} \rightarrow e_{aq}^- + H_2O \quad (k = 2.2 \times 10^{7} M^{-} s^{-}) \quad \text{Eq. (15)}$$

Based on the data presented in Fig. S5a, it can be seen that k_{obs} at

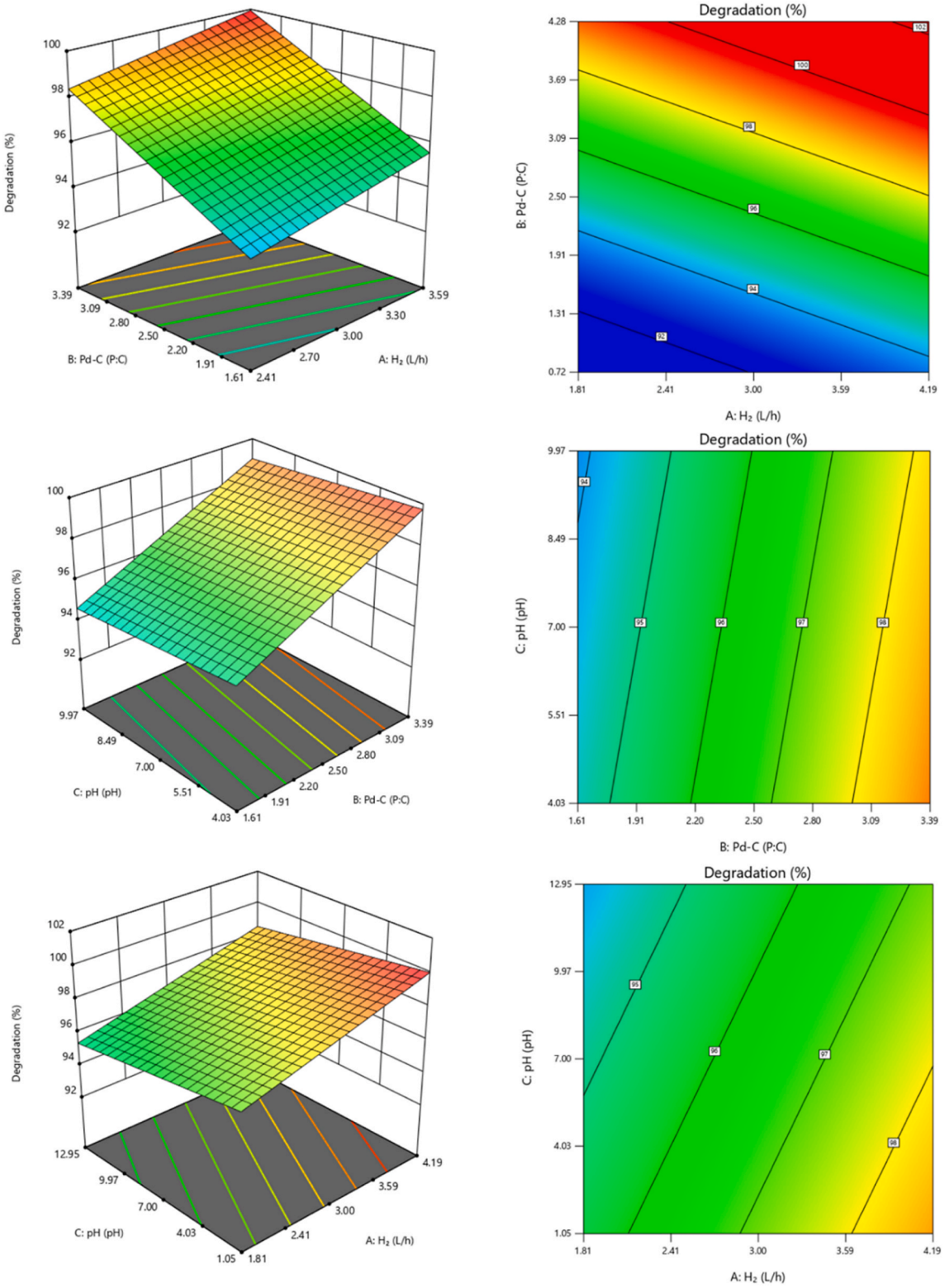

Fig. 4. 3D response surface and contour plot of CHL degradation efficiency using the optimized UV/Pd-C/H_2 process photocatalyst, (a) H_2 with Pd-C, (b) Pd-C with pH, and (c) H_2 with pH.

acidic pH is almost similar to the neutral solution, while alkaline conditions (pH 12) exhibited small k_{obs} (0.0626 min^{-1}), however after 30 min, complete degradation and dechlorination >82% (Fig. S5b) was obtained.

Thus, the observed pH effect of CHL degradation in acidic and basic media suggested that the degradation was higher at pH 2, 4 and 10, while pH 7 showed almost similar degradation effectiveness. This could be due to that at neutral pH the quantity of H^+ is much lower than in acidic conditions, while simultaneously, the e^-_{aq} stability and accumulation remained limited compared to alkaline condition. Therefore, the overall reactivity was slightly lower compared to acidic or basic conditions (Moussavi and Rezaei, 2017). Yoon et al. (2014) studied the ARP

based process for degradation of 1,2-DCA, it was observed that pH 4.65 and 10.6 possessed high degradation effectiveness than pH 7.2. In other study, slightly lower PFOA removal was observed at pH 7 compared acidic and alkaline environment (He et al., 2024). Lai et al., 2022 degraded an isoproturon via UV/PS process and observed lower k_{obs} at neutral condition in comparison to pH 6 and 8. While, in case of basic medium the presence of $^{-}$OH ions help to form the $^{\bullet}$OH radicals, hence these radicals contribute to speed up the reaction. However, at pH 12, the number of H^{+} is very small and may inhibit the degradation of CHL by scavenging the $H^{\bullet}$ radicals. Thus, in case of pH 12 rate of degradation decreased slightly. Furthermore, the surface charge of the Pd-C was slightly pH-dependent and determined via its point of zero charge (PZC). The surface was neutral or exhibited minimal electrostatic interactions with the CHL around neutral pH. This condition could decrease the adsorption effectiveness of CHL on the Pd-C catalyst surface, which was important for electron or radical-mediated interactions. The PZC values of Pd-C catalyst were close to neutrality at pH 6 – 7 and around pH 12, where the surface charge was minimal. The adsorption of CHL was weak and the degradation effectiveness was low under these pH conditions. On the other hand, at an acidic pH (2 – 4), the Pd-C surface was positively charged which enhanced the generation of $H^{\bullet}$ radicals and improved degradation (Rossmeisl et al., 2016; Guo et al., 2023, 2024). Whereas, negative charge was present on the surface at a moderately alkaline pH 10, which could facilitated the formation of reactive species i.e., $^{\bullet}$OH radicals and increased performance via enhancing interactions with CHL. These observations exhibited that degradation effectiveness was better when the pH was away from the PZC, and that conditions near to the PZC slowed down the process.

3.3.3.2. Effect of catalyst dose. The effect of increasing the molar ratio of Pd-C to CHL on degradation can be analyzed based on catalytic activity, availability of reactive sites, and the efficiency of hydrogen activation. Fig. S6a depicts the observed degradation and dechlorination of CHL at various Pd-C dosages (Fig. S6b). As the catalyst dosages increased, larger number of active sites were present that enhanced the reductants formation. Thus, the degradation rates of CHL enhanced significantly by the UV/Pd-C/H_2 process, which suggested the reduction of CHL could be promoted with the elevated Pd-C concentrations in the range of Pd-C:CHL = 1:2 to 4:2 mass ratio. It observed that Pd-C quantities boosted radical production.

3.3.3.3. Effect of hydrogen gas flow. The concentration of reducing agent utilized in ARPs is very important component controlling the reduction effectiveness. In the developed system, the reductant is continuously supplied in a form of gas flow. Hydrogen is provided in an excess, as only some part is dissolved in the aqueous phase. The effect of H_2 flow rate on the degradation of CHL in a UV/Pd-C/H_2 system is critical, as it directly influences the availability of hydrogen for catalytic reduction at given conditions of 20 mg/L CHL, Pd-C:CHL = 2:2 mass ratio and pH = 7. Fig. 5 shows that at low H_2 flow rates, the availability of hydrogen for catalytic activation on Pd-C is limited. Thus, the reactive hydrogen ($H^{\bullet}$) production is insufficient to meet the degradation demand. H_2 has a very low solubility in water at standard conditions - it is approximately 0.00157 g/L (Wiebe and Gaddy, 1934; Chabab et al., 2024). Hence, it is necessary to select optimal flow rates to maximize degradation efficiency by ensuring sufficient hydrogen activation and catalyst utilization. Results showed that with increasing gas flow larger number of $H^{\bullet}$ is formed which cause faster the degradation, such as, 3 L/h exhibited better outcomes compared to 2 L/h, while 4 L/h possessed superior results as predicted by CCD model. Hence, 4 L/h was selected as optimal for degradation. A complete degradation and dechlorination (Fig. S7) obtained was in 10 min and 60 min respectively.

However, for specific studies reported in next paragraphs, a lower flow rate of 2 L/h was purposefully selected. This enabled for a better understanding of mechanistic pathways under limiting conditions and

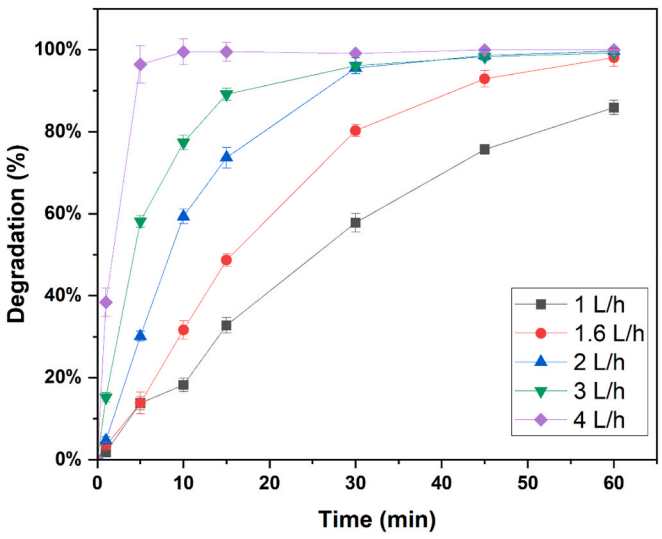

Fig. 5. Effects of hydrogen gas flow on degradation rates through the UV/Pd-C/H_2 process. Conditions of 20 mg/L CHL, Pd-C:CHL = 2:2 and pH = 7.

avoided fast degradation at higher flowrates of H_2 (high flow minimize small effects). Under laboratory scale experiments high ratio of H_2/treated solution is easily possible, while in process scale such need must be evaluated. Thus, knowledge about limitations taking place depending on water matrix are highly important.

3.3.3.4. Effect of coexisting ions and humic acids on the reduction of CHL. Wastewater comprises a considerable quantity of inorganic ionic species. Consequently, a reduction method should degrade target contaminants effectively and selectively in the occurrence of inorganic anions. Chloride (Cl^{-}) ions did not significantly affect CHL degradation. This could be attributed to its weak interaction with reductive species. Whereas, slight decrease in rate of reaction by inhibiting the active sites of catalyst (Zhao et al., 2017). Carbonate and sulfate ions showed slightly higher rate of reaction than control system, and complete degradation was observed with these anions (Rayaroth et al., 2023). While, this could also be stated carbonate and sulfate has low reactivity with e^{-}_{aq} and $H^{\bullet}$ (V Buxton et al., 1988). The effect was observed at CHL to anion of 1:10 M ratio. The research conducted under specifically suboptimal selected process conditions (to further understand the effect in the reaction mechanism by limiting the $H^{\bullet}$) such as CHL: 20 mg/L, H_2: 2 L/h, Pd-C:CHL = 4:2 mass ratio and pH 7, revealed that the existence of nitrate ions in the CHL solution has a negligible effect on the reduction of CHL (Fig. 6a). Reductants and anionic ions interaction slightly decreases CHL reduction effectiveness. The examination suggested that presence of ions in the solution have a lesser influence on CHL degradation in the developed ARP process. Meanwhile many effective procedures, for instance persulfate-based, diminish in the occurrence of inorganic ions, contaminant degradation effectiveness in actual conditions is much lower than in model solutions (Zhao et al., 2025).

The controlled organic matter content of the CHL solution was simulated by humic acid sodium salts (HASS), under same conditions as anions effect. CHL was completely reduced even in the presence of HASS. It is suggested that HASS acts as electron transfer mediator leading to enhanced production of reductants (Zhu et al., 2000; Liao et al., 2015; Page et al., 2012).

3.4. Identification of reductive radical species

Based on our experimental CHL degradation results and spectroscopic analysis, the effective CHL degradation in UV/Pd-C/H_2 and UV/S/Pd-C/H_2 and other systems could be ascribed to the generation of e^{-}_{aq} and $H^{\bullet}$. These radicals ($H^{\bullet}$ and e^{-}_{aq}) serves as the reducing agents in the

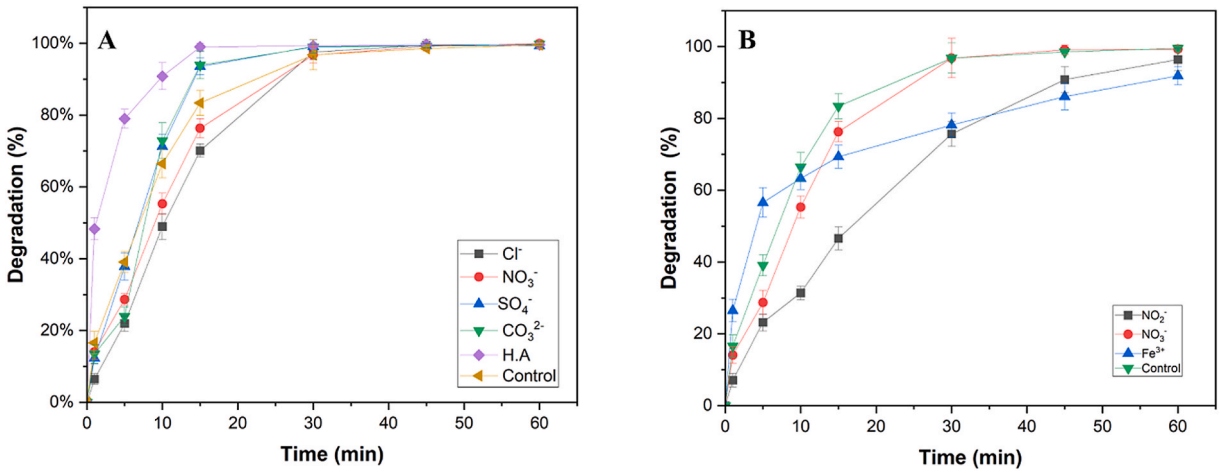

Fig. 6. (A) The effect of anions and (b) scavenger presence on the reduction of 20 mg/L CHL solution (CHL: anions molar ratio 1:10).

catalytic hydrogenation process, which then reduces CHL by breaking the C–Cl bond (Xu et al., 2013a, 2013b, 2016). The molar ratio of CHL to scavenger was set as 1:10 to ensure the effective quenching of radicals.

The analysis of the impact of $H^{\bullet}$ and e^{-}_{aq} radicals on CHL degradation in the UV/Pd-C/H_2 process, iron (III) cations (Fe^{3+}), NO_3^- and NO_2^- were selected as scavengers which then effectively quenched these reductive radicals according to reactions (Eqs. (16)–(21)). It was reported that NO_2^- and NO_3^- possess good scavenging properties for e^{-}_{aq} (Eqs. (18) and (20)) (Yu et al., 2021; Gu et al., 2016), however, only NO_2^- is capable for quenching $H^{\bullet}$ dominantly (Eq. (19)) (Yu et al., 2021).

$$Fe^{3+} + e^{-}_{aq} \rightarrow Fe^{2+} \quad (k = 5.2 \times 10^{9} M^{-} s^{-}) \qquad \text{Eq. (16)}$$

$$Fe^{3+} + H^{\cdot} \rightarrow Fe^{2+} + H^{+} \quad (k < 2 \times 10^{6} M^{-} s^{-}) \qquad \text{Eq. (17)}$$

$$NO_2^- + e^{-}_{aq} \rightarrow NO_2^{2-} \quad (k = 4.1 \times 10^{9} M^{-} s^{-}) \qquad \text{Eq. (18)}$$

$$NO_2^- + H^{\cdot} \rightarrow NO^{\cdot} + OH^{-} \quad (k = 7.1 \times 10^{8} M^{-} s^{-}) \qquad \text{Eq. (19)}$$

$$NO_3^- + e^{-}_{aq} \rightarrow (NO_3)^{2-} \quad (k = 9.7 \times 10^{9} M^{-} s^{-}) \qquad \text{Eq. (20)}$$

$$NO_3^- + H^{\cdot} \rightarrow NO_2^- + OH^{-} \quad (k = 1.4 \times 10^{6} M^{-} s^{-}) \qquad \text{Eq. (21)}$$

For instance, $H^{\bullet}$ may predominate in reaction with NO_2^- and generate $NO^{\bullet}$ or HNO_2 (Eq. (19)), which is confirmed by the k_{obs} of CHL in presence of NO_2^- (0.0506 min^{-1}) compared to controlled system (k_{obs} = 0.1196 min^{-1}) as shown in Fig. 5b. While, e^{-}_{aq} reacted faster with NO_3^- and Fe^{3+} compared to $H^{\bullet}$. CHL in presence of NO_3^- corresponding rate constant was 0.0835 min^{-1}, and it exhibited no significant quenching effect and yield almost similar degradation as controlled system. Although, this effect could be explained by examining the both rate constants and concentration of ionic species in the solution. At the pH = 4, the hydronium ion (proton) concentration was $[H^+] \approx 10^{-4}$ M, while, $[NO_3^-] \approx 9.4 \times 10^{-4}$ M at CHL:scavenger = 1:10 M ratio. Importantly, Eq. (14) demonstrates the rate constant of e^{-}_{aq} with H^+ (2.3×10^{10} M^{-} s^{-}), which is higher than rate constant of NO_3^- with e^{-}_{aq} (Eq. (20)), hence NO_3^- quenching effect did not show strong inhibition. On the other hand, protonation lead to effective conversion of e^{-}_{aq} in $H^{\bullet}$, which significantly decreased the concentration of produced e^{-}_{aq}, which could react with NO_3^-. Additionally, NO_3^- did not effectively reduce the degradation due to slow interaction with $H^{\bullet}$ (Eq. (21)). Moreover, in previous studies of UV/SO_3^{2-} system have demonstrated that acidic conditions favour $H^{\bullet}$ radicals formation owing to rapid protonation of e^{-}_{aq}, whereas, alkaline and neutral conditions promote e^{-}_{aq} presence (Wu et al., 2023). According to Xiao et al. (2017), in UV/SO_3^{2-} process for reduction of bromate, the active radicals at pH 4 and 9 were $H^{\bullet}$, and e^{-}_{aq} respectively, while at pH 7 their coexistence was obtained, and the effect of NO_3^- at pH 4 was negligible on degradation inhibition which confirmed the $H^{\bullet}$ radical dominant role. These results confirmed with the reported kinetics and suggested that $H^{\bullet}$ radicals were responsible for CHL degradation, whereas e^{-}_{aq} had a supporting role.

Furthermore, the quenching effect of using Fe^{3+} (Eqs. (16) and (17)), the degradation efficiency of CHL was declined from 99.9 to 91.9% after 60 min and the depletion of Fe^{3+} (CHL k_{obs} = 0.1051 min^{-1}) in the solution is clearly visible as the yellow colored Fe^{3+} transformed into colorless Fe^{2+} upon reaction with reductants, ensuing in the decolorization of the solution (Li et al., 2020; Lin et al., 2021; Cichocki et al., 2024).

Moreover, by comparing the rate of reactions of controlled process with NO_3^- and NO_2^- quenching anionic species, the presence of $H^{\bullet}$ and e^{-}_{aq} were responsible for CHL degradation (Fig. 6b). As there was no big drop in CHL degradation for NO_3^- presence, it means there was no direct contribution of e^{-}_{aq}, while, Fe^{3+} and NO_2^- found to be the most effective scavenger which decreased the reductant radicals effectiveness, as NO_2^- has high rate constant with $H^{\bullet}$ radical. These observations suggested that $H^{\bullet}$ was a dominant radical responsible for CHL degradation.

On the other hand, UV can form $^{\bullet}OH$ radicals, thus, to observe the effect of these radicals to CHL degradation, a CHL to MeOH molar ratio of 1:10 was used to ensure the effective quenching of radicals. As shown in Fig. S8, there is no major difference between the control system and with the control system + MeOH and UV sole with MeOH was also compared with UV sole process. Thus, these scavenging experiments confirmed that there is no major effect of $^{\bullet}OH$ radicals in CHL degradation.

3.5. *Computational predication and insights into the degradation mechanism of CHL*

Fukui indices in Table 2S suggest that C11 (as indicated in Fig. S9) has the highest reactivity towards radical attack, followed by N15 and C10. These data agree with the proposed formation of the cyclo-chloro species. This is thought to be caused by radical attack of $H^{\bullet}$ to the C10–C11 bond and the hydrogenolysis of the N15–C10 bond from radical attack by e^{-}_{aq}. Atoms C14, C13, and N15 have large Fukui indices, suggesting high reactivity at those sights and supporting the proposed formation of 4-methylaniline and N,N-dimethylformamide due to hydrogenolysis of the Cl4–C13 and the N15–C17 bonds via attack from e^{-}_{aq}.

On the other hand, catalytic reduction reactions play a major role in modern chemistry and are often based on hydrogen gas as a reducing agent. In catalytic hydrogenation, the reduction occurs on the surface of a metal catalyst. The H_2 molecules dissociate into hydrogen radical ($H^{\bullet}$)

on the metal surface. H_2 and CHL are adsorbed onto the surface of the metal catalyst. The $H^{\bullet}$ reacts with the CHL, replacing the chlorine atom with a hydrogen atom, forming the reduced product and releasing HCl (Eq. (22)).

$$CHL + H^{\cdot} \rightarrow CHL^{\cdot} + Cl^{-} \quad \text{(Eq. 22)}$$

Based on the results of GC-MS analyses for individual samples taken during the herbicide degradation process, we proposed a tentative mechanism for the degradation of CHL to simple organic molecules. The chemical bonds most susceptible to hydrogenolysis are marked in blue in Fig. S10. The degradation process was typically initiated by C–Cl bond activation and reductive dechlorination, which represented the dominant pathway.

Our observations show that the discussed degradation process proceeds along two basic paths. The first one leading to the formation of 1-chloro-2-methylcyclohexa-1,3-diene as a key intermediate can lead via two alternative mechanisms: i.e. with partial reduction of the aromatic system, leading to compound 1 (Fig. 7) containing an allylamine system. The process of reduction of the aromatic system, although difficult, is not excluded in the presence of a palladium catalyst and the potential possibility of tautomerization of the reduced fragment to an imine (from C=C-NH_2 to HC-C=NH), which undergoes hydrogen addition much more easily. The second, less probable subpath of the process assumes the initial hydrogenolysis of the C-N bond between the aryl fragment and the urea part and then the addition of hydrogen to the aromatic system of o-chlorotoluene. In both cases, the processes lead to the formation of 1-chloro-2-methylcyclohexa-1,3-diene (2) whose presence is manifested in the MS spectrum as a signal at 128 m/z accompanied by a M+2 signal at 130 m/z with an intensity of 33%, clearly indicating the presence of one chlorine atom in the intermediate molecule after degradation.

A different way of CHL degradation proceeds with hydrogenolysis of the C-N bond between the carbonyl carbon atom and the urea nitrogen atom. This process must be accompanied by simultaneous hydrogenolysis of the carbon-chlorine bond, resulting in the formation of p-toluidine observed in the MS spectrum as a signal of 107 m/z (3). During this process, N,N-dimethylformamide (4) 73 m/z is formed in parallel, its formation also requires hydrogenolysis of the C-N bond between the carbonyl carbon atom and the urea nitrogen atom, however, hydrogenolysis of the carbon-chlorine bond is not necessary as shown in Fig. 7.

Moreover, previously reported studies have shown that degradation pathways exhibit numerous reaction pathways commonly coexist, where primary dehalogenation is followed by secondary changes. Haque et al. (2006) studied the photocatalytic degradation of CHL in aqueous TiO_2 suspensions, and observed the C-N cleavage between carbonyl carbon and nitrogen atoms, which formed a 3-chloro-4-methylphenylamine. Similarly, Boulkamh et al. (2001) investigated the photochemical degradation behavior of metoxuron herbicide, which followed the photohydrolysis of C-Cl bond as a primary pathway, and N-demethylation involved the C-N bond as a minor pathway, obtained via methyl

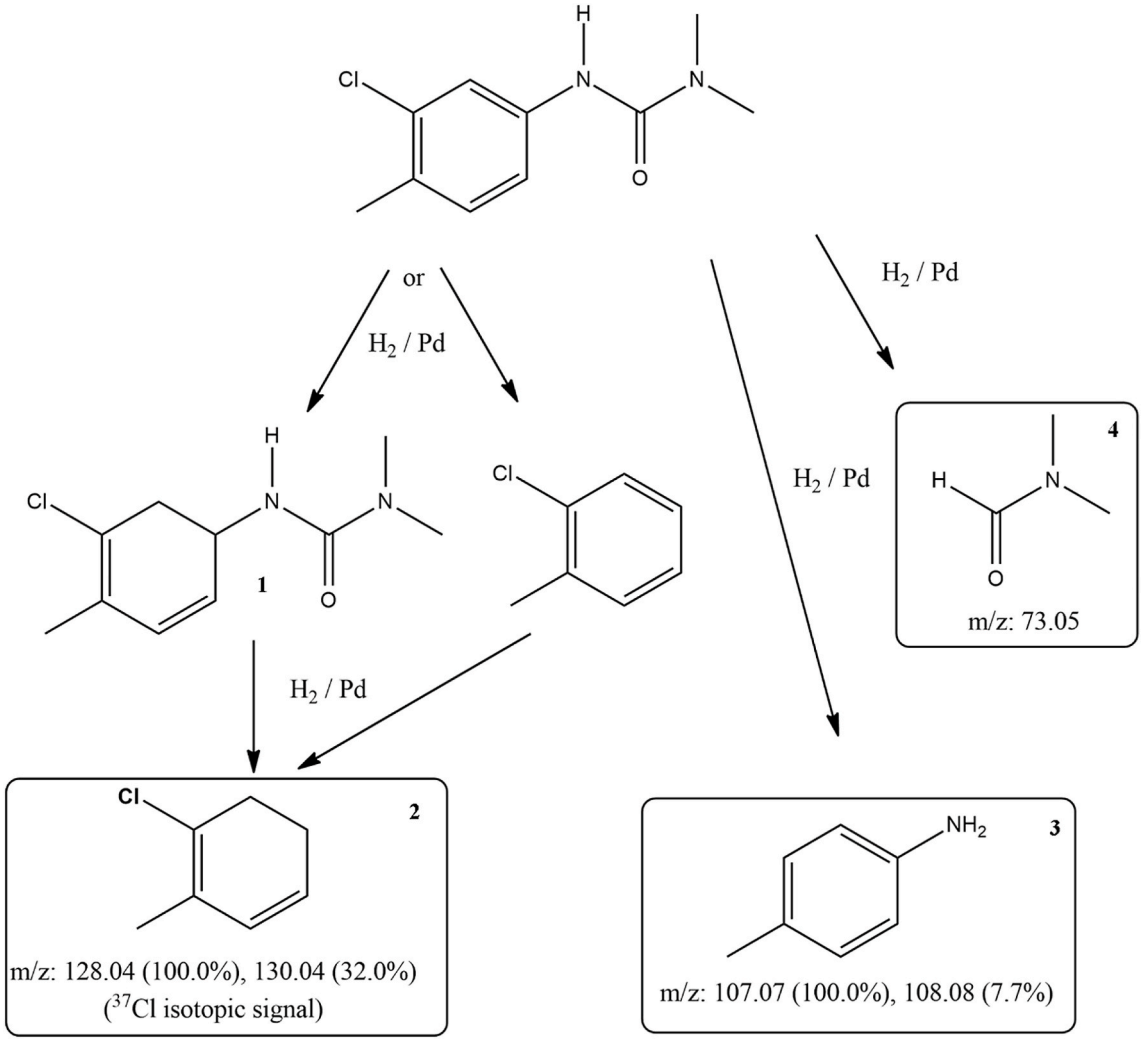

Fig. 7. The proposed degradation pathway of CHL via UV/Pd-C/H_2 process. Compounds marked by a frame were identified in process samples based on MS spectra.

enolate intermediate followed by elimination of methanol.

We based the proposal of the course of the observed process on the observation of several sufficiently stable intermediates, it is not excluded that additional chemical reactions also occur in the discussed process, and what is obvious, subsequent degradations of the observed intermediates must also occur.

3.6. Reusability of Pd-C catalyst

Reusability of catalyst is an economic subject. The reusability and stability of Pd-C was significant for evaluating the catalyst performance. CHL degradation process was performed for 1 h, later the Pd-C catalyst was collected carefully after 1st cycle via the vacuum filtration assembly from the reactor assembly and applied for next degradation cycle. In the reusability Pd-C catalyst exhibited no major loss/slight loss in catalytic activity. The catalyst drops certain activity between cycles 1st and 5th from 100% to 89.4% respectively (Fig. S11), which represents concentration profiles for all five runs in consecutive order.

Here, super activity of Pd-C was observed in the first run which often benefits from the catalyst's original surface, which provides a maximum number of active sites because there are no reaction intermediates, by-products, or impurities initially blocking the sites, enabling maximum performance. This behavior of fresh catalyst had been widely explored, where catalyst surface facilitates optimal interaction for substrate (Gómez-Quero et al., 2008; Keane, 2011). Zhang et al. (2022) tested the stability of nano-Fe/Pd-C catalyst, and catalyst activity was decreased to 84.4% after 5th cycle, although the SEM and XRD confirmed structural stability of catalyst. They attributed this inhibition due to coke deposition on catalyst surface. In other study, reusability of Pd-C catalyst showed decrease in conversion of p-bromoanisol around 78% after 3rd cycle (Alshammari et al., 2021). Similarly, CNT-Pd catalyst demonstrated accumulation of intermediates on the catalyst surface which decreased reaction effectiveness, however, synthesized catalyst exhibited stable morphology (Kim et al., 2016). Moreover, studies on deactivation of catalyst owing to fouling of active Pd sites, Pd NPs sintering, and pore clogging of Pd-C have been widely explored, while, the SEM and XRD confirmed the stability of catalyst after reusability (Chen et al., 2015; Wang et al., 2013; Jing et al., 2025; Dong et al., 2015). After the initial super activity, the catalyst settles into a state where it delivered consistent performance over time. For example, fouling of a catalyst may formed a surface layer of reaction intermediates (e.g., adsorbed molecules) that decreased the number of exposed sites but did not deactivate the catalyst entirely, thus, allowed the Pd-C to stabilize at a slightly lower but steady activity level. Thus, such fouling induces the incomplete deactivation by adsorbed intermediates has been observed in supported Pd catalysts in hydrodechlorination processes without fully inhibiting the catalytic activity (Köhler et al., 2002). Also, the AC support itself might experience pore clogging due to by-products or large molecules, which restricted access to embedded Pd NPs. Ioannidou et al. (2016) performed cyclability test on BPA which decreased from 100% to 74% after 5 cycles. The methyl orange degradation rate constants of hydrogenated titania decreased four time after three reuse (Saputera et al., 2015). While, when platinum was added to titania, this loss of activity was about 1.6 times less.

Despite subjected to several repetitive processes, the Pd-C catalyst remained stable and active during the degradation of CHL, ensuring its excellent performance. Also, it was noticed the Pd-C catalyst could be used for further cyclability processes due to its stable, steady nature in shear conditions. Thus, according to SEM and XRD, the overall structure of Pd-C catalyst remained nearly similar and the effectiveness from superior catalyst activity to stable lower activity was attributed to combined effect of fouling of active Pd sites and pore clogging of AC.

3.7. Leaching of Pd

ICP-OES was utilized to control the Pd leaching in the reaction mixture. Pd quantity in CHL samples was not detected by ICP-OES (signal below LOD). This corresponded to low leaching estimated as below 1.78% of the starting Pd-amount.

Furthermore, the presence of Pd in EDS spectra after cycles confirmed the surface retention of Pd NPs. However, ICP-OES analysis indicated minor Pd leaching over time. Thus, it could be evaluated that the combination of EDS and ICP-OES supported the conclusion that there is no major active material loss occurred, a significant portion of the Pd remains immobilized on the support surface, maintained catalytic activity. Moreover, SEM images of catalyst surface of fresh, 1st and 5th cycles were found to possess almost similar morphology as discussed earlier. XRD results confirmed the characteristic diffraction peaks of Pd-C catalyst. Hence, it is suggested that based on obtained ICP-OES result and other supporting techniques Pd-C catalyst exhibited excellent stability.

3.8. Economic analysis

An economic evaluation was achieved using experimental information from this study and scaled from a treated volume of 1 L to 1 m^3, with an CHL concentration of 20 mg/L. Additionally, UV lamp was 450 W, hydrogen generator 230 W and peristaltic pump with 230 W. In the calculations we included that only 50% of maximum productivity of H_2 generator was used and 10% of peristaltic pump maximal flowrate. Thus, operating for 10 min results in an energy consumption of 0.07515, 0.01921 and 0.003841 kWh by UV lamp, H_2 generator and peristaltic pump respectively, with a cost of $0.03142.

Thus, the total expense of treating the 1 m^3 CHL solution with UV irradiation is $31.42/$m^3$. Moreover, it can be suggested that incident UV intensity is greater than 1 L solution, so it could be used in large volume solutions which eventually make system more cost-efficient.

Moreover, the reported 89% efficiency over five cycles provides a reliable stability for industrial application, indicating consistency over long time with suitable modifications. The complete effectiveness of the Pd-C catalyst in large wastewater treatment could be completed with further industrial investigating, improvements in catalyst support, and regeneration approaches. It is an attractive choice to companies seeking cost-effective and eco-friendly solutions due to its scalability, recyclability, and environmental benefits. In summary, treating CHL with UV irradiation costs $31.42/$m^3$, although it may be economically feasible for large-scale industries able of generating their own electricity.

However, the UV reactor system may be optimized to extensively reduce chemical and operating expenditures. UV/Pd-C/H_2 process design utilized a 450 W UV lamp that produced high light intensity, allowing the simultaneous treatment of large volumes of PUH's solution. This lamp could be suitable for treatment of 10–100 L batches at once, depending on how well UV light is utilized, as opposed to just 1 L in 10 min. This delivered the energy expense through a larger volume of pollutant water, decreasing the operational cost per liter.

Based on the catalyst investment cost the current market prices of 500 g of Pd-C is $6230. To treat 1 L of 20 mg/L solution, approximately 39.9 mg of Pd-C with a value of $0.485 was used per cycle. However, this catalyst is reused for 5 cycles so it cost around $0.097/cycle. This investment cost is one time purchase for the years of reusability of catalyst as happening in the industries.

Future considerations should focus on improving reactor designs and integrating renewable energy sources to further increase the economic sustainability of this process.

4. Conclusions

The studies revealed the first attempt of CHL reduction through photocatalytic hydrogenation, and shown highly reactive and efficient reduction reactions of UV/Pd-C/H_2-based ARP in the aqueous phase. Under optimal reaction conditions, this process achieved excellent dechlorination (94.1 %) and CHL degradation (99.4%) within 10 min.

The UV/Pd-C/H_2 method performed greatly with coexisting ions and presented remarkable reduction and dechlorination effectiveness from pH 2 to 12. The significant catalytic activity of the optimized Pd–C photocatalyst, which is obtained from AC, corresponds to its exceptional CHL degradation. This performance is accelerated by the large surface area, which improves band-gap tuning, charge carrier photogeneration, separation, and transport.

Finally, we can conclude, Pd-C photocatalytic hydrogenation, generated highly reactive and non-selective radicals ($H^{\bullet}$, e^{-}_{aq}) that quickly degraded persistent organic compound. This provided a more effective, low-byproduct, and eco-friendly way to treat PUHs.

Studies of degradation mechanism revealed that the CHL follows degradation via two basic paths. The first pathway involves partial reduction of aromatic system, forming 1-chloro-2-methylcyclohexa-1,3-diene, either via reduction – tautomerization – hydrogenation or by initial C-N bond hydrogenolysis followed by aromatic reduction. The second path, less probable subpath of the process, assumes the initial hydrogenolysis of the C-N bond between the aryl fragment and the urea part and then the addition of hydrogen to the aromatic system of chlorotoluene.

Additionally, Fukui indices suggested the formation of cyclo-chloro and other byproducts. Fukui indices support reactivity at C14-C13 and the N15-C17 bonds by the radical attack. Moreover, over five repetitive photocatalytic cycles, the crystalline structure, shape, physicochemical, and photocatalytic working of Pd-C did not change significantly. Based on quenching experiments of CHL degradation results suggested that $H^{\bullet}$ radical was dominant while, e^{-}_{aq} demonstrated indirect contribution, by supporting $H^{\bullet}$ radicals formation owing to rapid protonation of e^{-}_{aq} at acidic conditions. The complete degradation was obtained within 10 min at optimal conditions of 4 L/h of H_2, Pd-C:CHL = 4:2 ratio, acidic pH (4) and 20 mg/L CHL model solution.

Latest developments in ARP-based studies should focus on important concerns such as scalability, energy demand and operational costs under practical conditions. Pilot-scale experiments are significant for evaluating long-term operation in complex water matrices, and combining ARPs with renewable sources could enhance sustainability and cost effectiveness. These proposals are important for transforming laboratory innovations into real-world applications.

CRediT authorship contribution statement

Bakhtiar Ali Samejo: Conceptualization, Data curation, Investigation, Visualization, Writing – original draft. **Ar. M. Fonlon:** Software, Visualization. **John M. Herbert:** Resources, Software, Validation, Visualization. **Marcin Łapiński:** Investigation, Visualization. **Jakub Karczewski:** Resources, Writing – review & editing. **Sławomir Makowiec:** Conceptualization, Validation, Visualization. **Grzegorz Boczkaj:** Conceptualization, Funding acquisition, Investigation, Methodology, Project administration, Resources, Supervision, Validation, Writing – original draft, Writing – review & editing.

Declaration of competing interest

☒ J.M.H. is part owner of Q-Chem and serves on its board of directors.

Acknowledgements

The authors gratefully acknowledge financial support from the National Science Centre, Warsaw, Poland for project OPUS nr UMO-2021/41/B/ST8/01575. Work by Ar.M.F. and J.M.H. was supported by the U. S. National Science Foundation, grant no. CHE-2402361.

Appendix A. Supplementary data

Supplementary data related to this article can be found online at https://doi.org/10.1016/j.jenvman.2026.130150.

Data availability

No data was used for the research described in the article.

References

Abdelhameed, R.M., El-Medani, S.M., Elantabli, F.M., El-Shahat, M., 2024. Uses of Palladium Complexes in Accelerating Chemical Reactions Under Visible Light Irradiation.

Alshammari, H.M., Aldosari, O.F., Alotaibi, M.H., Alotaibi, R.L., Alhumaimess, M.S., Morad, M.H., Adil, S.F., Shaik, M.R., Islam, M.S., Khan, M., Alwarthan, A., 2021. Facile synthesis and characterization of palladium@carbon catalyst for the suzuki-miyaura and mizoroki-heck coupling reactions. Appl. Sci. 11. https://doi.org/10.3390/app11114822.

Badawi, N., Rønhede, S., Olsson, S., Kragelund, B.B., Johnsen, A.H., Jacobsen, O.S., Aamand, J., 2009. Metabolites of the phenylurea herbicides chlorotoluron, diuron, isoproturon and linuron produced by the soil fungus mortierella sp. Environ. Pollut. 157, 2806–2812. https://doi.org/10.1016/J.ENVPOL.2009.04.019.

Bayuo, J., Abukari, M.A., Pelig-Ba, K.B., 2020. Optimization using central composite design (CCD) of response surface methodology (RSM) for biosorption of hexavalent chromium from aqueous media. Appl. Water Sci. 10, 135. https://doi.org/10.1007/s13201-020-01213-3.

Benitez, F.J., Real, F.J., Acero, J.L., Garcia, C., 2006. Photochemical oxidation processes for the elimination of phenyl-urea herbicides in waters. J. Hazard. Mater. 138, 278–287. https://doi.org/10.1016/J.JHAZMAT.2006.05.077.

Benitez, F.J., Real, F.J., Acero, J.L., Garcia, C., 2007a. Kinetics of the transformation of phenyl-urea herbicides during ozonation of natural waters: rate constants and model predictions. Water Res. 41, 4073–4084. https://doi.org/10.1016/J.WATRES.2007.05.041.

Benitez, F.J., Real, F.J., Acero, J.L., Garcia, C., Llanos, E.M., 2007b. Kinetics of phenylurea herbicides oxidation by fenton and photo-Fenton processes. J. Chem. Technol. Biotechnol. 82, 65–73. https://doi.org/10.1002/jctb.1638.

Bezerra, M.A., Santelli, R.E., Oliveira, E.P., Villar, L.S., Escaleira, L.A., 2008. Response surface methodology (RSM) as a tool for optimization in analytical chemistry. Talanta 76, 965–977. https://doi.org/10.1016/J.TALANTA.2008.05.019.

Boulkamh, A., Harakat, D., Sehili, T., Boule, P., 2001. Phototransformation of metoxuron [3-(3-chloro-4-methoxyphenyl)-1,1-dimethylurea] in aqueous solution. Pest Manag. Sci. 57, 1119–1126. https://doi.org/10.1002/ps.405.

Cako, E., Darvishi Cheshmeh Soltani, R., Sun, X., Boczkaj, G., 2022. Desulfurization of raw naphtha cuts using hybrid systems based on Acoustic cavitation and advanced oxidation processes (AOPs). Chem. Eng. J. 439, 135354. https://doi.org/10.1016/J.CEJ.2022.135354.

Chabab, S., Kerkache, H., Bouchkira, I., Poulain, M., Baudouin, O., Moine, É., Ducousso, M., Hoang, H., Galliéro, G., Cézac, P., 2024. Solubility of H2 in water and NaCl brine under subsurface storage conditions: measurements and thermodynamic modeling. Int. J. Hydrogen Energy 50, 648–658. https://doi.org/10.1016/J.IJHYDENE.2023.10.290.

Chai, J.-D., Head-Gordon, M., 2008. Long-range corrected hybrid density functionals with damped atom–atom dispersion corrections. Phys. Chem. Chem. Phys. 10, 6615–6620. https://doi.org/10.1039/B810189B.

Chaplin, B.P., Reinhard, M., Schneider, W.F., Schüth, C., Shapley, J.R., Strathmann, T.J., Werth, C.J., 2012. Critical review of Pd-Based catalytic treatment of priority contaminants in water. Environ. Sci. Technol. 46, 3655–3670. https://doi.org/10.1021/es204087q.

Chen, H., He, Y., Pfefferle, L.D., Pu, W., Wu, Y., Qi, S., 2018. Phenol catalytic hydrogenation over palladium nanoparticles supported on metal-organic frameworks in the aqueous phase. ChemCatChem 10, 2558–2570. https://doi.org/10.1002/cctc.201800211.

Chen, H., Xu, Z., Wan, H., Zheng, J., Yin, D., Zheng, S., 2010. Aqueous bromate reduction by catalytic hydrogenation over Pd/Al2O3 catalysts. Appl. Catal., B 96, 307–313. https://doi.org/10.1016/J.APCATB.2010.02.021.

Chen, T., Li, D., Jiang, H., Xiong, C., 2015. High-performance Pd nanoalloy on functionalized activated carbon for the hydrogenation of nitroaromatic compounds. Chem. Eng. J. 259, 161–169. https://doi.org/10.1016/J.CEJ.2014.07.054.

Chen, X., Xiaohui, W., Fang, D., 2020. A review on C1s XPS-Spectra for some kinds of carbon materials, fullerenes, nanotubes and. Carbon Nanostructures 28, 1048–1058. https://doi.org/10.1080/1536383X.2020.1794851.

Chen, Z., Teng, Y., Wang, W., Hong, R., Huang, L., Wang, X., Zhu, F., Li, H., Hao, S., Wu, B., Gu, C., 2022. Enhanced UV photoreductive destruction of perfluorooctanoic acid in the presence of alcohols: synergistic mechanism of hydroxyl radical quenching and solvent effect. Appl. Catal., B 316, 121652. https://doi.org/10.1016/J.APCATB.2022.121652.

Cho, H.-J., Chen, V.T., Qiao, S., Koo, W.-T., Penner, R.M., Kim, I.-D., 2018. Pt-Functionalized PdO nanowires for room temperature hydrogen gas sensors. ACS Sens. 3, 2152–2158. https://doi.org/10.1021/acssensors.8b00714.

Chu, R., Khan, Z.U.I.H., Zhu, Y., Zhao, R., Wu, W., Sun, J., 2025. Theoretical simulation degradation of bromoxynil by ozonation in liquid phase: mechanism pathways, kinetics, and ecotoxicity. Int. J. Quant. Chem. 125, e70041. https://doi.org/10.1002/qua.70041.

Cichocki, Ł., Kong, L., Wang, C., Przyjazny, A., Boczkaj, G., 2024. First highly effective non-catalytic nitrobenzene reduction in UV/dithionite system with aniline

production – advanced reduction process (ARP) approach. Chem. Eng. J. 479, 147878. https://doi.org/10.1016/J.CEJ.2023.147878.
Conrad, H., Ertl, G., Latta, E.E., 1974. Adsorption of hydrogen on palladium single crystal surfaces. Surf. Sci. 41, 435–446. https://doi.org/10.1016/0039-6028(74)90060-0.
Crawford, C.J., Qiao, Y., Liu, Y., Huang, D., Yan, W., Seeberger, P.H., Oscarson, S., Chen, S., 2021. Defining the qualities of high-quality palladium on carbon catalysts for hydrogenolysis. Org. Process Res. Dev. 25, 1573–1578. https://doi.org/10.1021/acs.oprd.0c00536.
Cullington, J.E., Walker, A., 1999. Rapid biodegradation of diuron and other phenylurea herbicides by a soil bacterium. Soil Biol. Biochem. 31, 677–686. https://doi.org/10.1016/S0038-0717(98)00156-4.
Das, T.N., Huie, R.E., Neta, P., 1999. Reduction potentials of SO3•-, SO5•-, and S4O6•3- radicals in aqueous solution. J. Phys. Chem. A 103, 3581–3588. https://doi.org/10.1021/jp9900234.
Dong, Z., Le, X., Dong, C., Zhang, W., Li, X., Ma, J., 2015. Ni@Pd core–shell nanoparticles modified fibrous silica nanospheres as highly efficient and recoverable catalyst for reduction of 4-nitrophenol and hydrodechlorination of 4-chlorophenol. Appl. Catal., B 162, 372–380. https://doi.org/10.1016/j.apcatb.2014.07.009.
Elakiya, C., Shankar, R., Vijayakumar, S., Kolandaivel, P., 2017. A theoretical study on the reaction mechanism and kinetics of allyl alcohol (CH2 = CHCH2OH) with ozone (O3) in the atmosphere. Mol. Phys. 115, 895–911. https://doi.org/10.1080/00268976.2017.1292012.
Epifanovsky, E., Gilbert, A.T.B., Feng, X., Lee, J., Mao, Y., Mardirossian, N., Pokhilko, P., White, A.F., Coons, M.P., Dempwolff, A.L., Gan, Z., Hait, D., Horn, P.R., Jacobson, L. D., Kaliman, I., Kussmann, J., Lange, A.W., Lao, K.U., Levine, D.S., Liu, J., McKenzie, S.C., Morrison, A.F., Nanda, K.D., Plasser, F., Rehn, D.R., Vidal, M.L., You, Z.-Q., Zhu, Y., Alam, B., Albrecht, B.J., Aldossary, A., Alguire, E., Andersen, J. H., Athavale, V., Barton, D., Begam, K., Behn, A., Bellonzi, N., Bernard, Y.A., Berquist, E.J., Burton, H.G.A., Carreras, A., Carter-Fenk, K., Chakraborty, R., Chien, A.D., Closser, K.D., Cofer-Shabica, V., Dasgupta, S., de Wergifosse, M., Deng, J., Diedenhofen, M., Do, H., Ehlert, S., Fang, P.-T., Fatehi, S., Feng, Q., Friedhoff, T., Gayvert, J., Ge, Q., Gidofalvi, G., Goldey, M., Gomes, J., González-Espinoza, C.E., Gulania, S., Gunina, A.O., Hanson-Heine, M.W.D., Harbach, P.H.P., Hauser, A., Herbst, M.F., Hernández Vera, M., Hodecker, M., Holden, Z.C., Houck, S., Huang, X., Hui, K., Huynh, B.C., Ivanov, M., Jász, Á., Ji, H., Jiang, H., Kaduk, B., Kähler, S., Khistyaev, K., Kim, J., Kis, G., Klunzinger, P., Koczor-Benda, Z., Koh, J.H., Kosenkov, D., Koulias, L., Kowalczyk, T., Krauter, C.M., Kue, K., Kunitsa, A., Kus, T., Ladjánszki, I., Landau, A., V Lawler, K., Lefrancois, D., Lehtola, S., Li, R.R., Li, Y.-P., Liang, J., Liebenthal, M., Lin, H.-H., Lin, Y.-S., Liu, F., Liu, K.-Y., Loipersberger, M., Luenser, A., Manjanath, A., Manohar, P., Mansoor, E., Manzer, S.F., Mao, S.-P., V Marenich, A., Markovich, T., Mason, S., Maurer, S.A., McLaughlin, P.F., Menger, M. F.S.J., Mewes, J.-M., Mewes, S.A., Morgante, P., Mullinax, J.W., Oosterbaan, K.J., Paran, G., Paul, A.C., Paul, S.K., Pavošević, F., Pei, Z., Prager, S., Proynov, E.I., Rák, Á., Ramos-Cordoba, E., Rana, B., Rask, A.E., Rettig, A., Richard, R.M., Rob, F., Rossomme, E., Scheele, T., Scheurer, M., Schneider, M., Sergueev, N., Sharada, S.M., Skomorowski, W., Small, D.W., Stein, C.J., Su, Y.-C., Sundstrom, E.J., Tao, Z., Thirman, J., Tornai, G.J., Tsuchimochi, T., Tubman, N.M., Veccham, S.P., Vydrov, O., Wenzel, J., Witte, J., Yamada, A., Yao, K., Yeganeh, S., Yost, S.R., Zech, A., Zhang, I.Y., Zhang, X., Zhang, Y., Zuev, D., Aspuru-Guzik, A., Bell, A.T., Besley, N.A., Bravaya, K.B., Brooks, B.R., Casanova, D., Chai, J.-D., Coriani, S., Cramer, C.J., Cserey, G., DePrince III, A.E., DiStasio Jr., R.A., Dreuw, A., Dunietz, B. D., Furlani, T.R., Goddard III, W.A., Hammes-Schiffer, S., Head-Gordon, T., Hehre, W.J., Hsu, C.-P., Jagau, T.-C., Jung, Y., Klamt, A., Kong, J., Lambrecht, D.S., Liang, W., Mayhall, N.J., McCurdy, C.W., Neaton, J.B., Ochsenfeld, C., Parkhill, J.A., Peverati, R., Rassolov, V.A., Shao, Y., V Slipchenko, L., Stauch, T., Steele, R.P., Subotnik, J.E., Thom, A.J.W., Tkatchenko, A., Truhlar, D.G., Van Voorhis, T., Wesolowski, T.A., Whaley, K.B., Woodcock III, H.L., Zimmerman, P.M., Faraji, S., Gill, P.M.W., Head-Gordon, M., Herbert, J.M., Krylov, A.I., 2021. Software for the frontiers of quantum chemistry: an overview of developments in the Q-Chem 5 package. J. Chem. Phys. 155, 084801. https://doi.org/10.1063/5.0055522.
Federico, C., Motta, S., Palmieri, C., Pappalardo, M., Librando, V., Saccone, S., 2011. Phenylurea herbicides induce cytogenetic effects in Chinese hamster cell lines. Mutat. Res. Genet. Toxicol. Environ. Mutagen 721, 89–94. https://doi.org/10.1016/J.MRGENTOX.2010.12.013.
Fedorov, K., Wang, C., Shah, N.S., Boczkaj, G., 2025. Boosting the radical-induced reductive degradation of clofibric acid in water: synergistic effect of SO32−/UV and hydrodynamic cavitation (HC). J. Environ. Manag. 391, 126506. https://doi.org/10.1016/J.JENVMAN.2025.126506.
Franch, C., Rodríguez-Castellón, E., Reyes-Carmona, Á., Palomares, A.E., 2012. Characterization of (sn and Cu)/Pd catalysts for the nitrate reduction in natural water. Appl. Catal. Gen. 425–426, 145–152. https://doi.org/10.1016/J.APCATA.2012.03.015.
Fuentealba, P., Pérez, P., Contreras, R., 2000. On the condensed Fukui function. J. Chem. Phys. 113, 2544–2551. https://doi.org/10.1063/1.1305879.
Fujimoto, A., Yamada, Y., Koinuma, M., Sato, S., 2016. Origins of sp3C peaks in C1s X-ray photoelectron spectra of carbon materials. Anal. Chem. 88, 6110–6114. https://doi.org/10.1021/acs.analchem.6b01327.
Gatidou, G., Stasinakis, A.S., Iatrou, E.I., 2015. Assessing single and joint toxicity of three phenylurea herbicides using Lemna minor and Vibrio fischeri bioassays. Chemosphere 119, S69–S74. https://doi.org/10.1016/J.CHEMOSPHERE.2014.04.030.
Gómez-Quero, S., Cárdenas-Lizana, F., Keane, M.A., 2008. Effect of metal dispersion on the liquid-phase hydrodechlorination of 2,4-Dichlorophenol over Pd/Al2O3. Ind. Eng. Chem. Res. 47, 6841–6853. https://doi.org/10.1021/ie0716565.
Gonçalves, R.A., Kuznetsov, A., Ciapina, E.G., Quade, A., Teodoro, M.D., Baldan, M.R., Berengue, O.M., 2023. Insights into the origin of the enhanced electrical conductivity of Pd-Sb2O3 nanoparticles: a combined experimental and theoretical study. J. Alloys Compd. 933, 167667. https://doi.org/10.1016/j.jallcom.2022.167667.
Gu, J., Yang, L., Ma, J., Jiang, J., Yang, J., Zhang, J., Chi, H., Song, Y., Sun, S., Tian, W. Q., 2017. Hydrated electron (Eaq−) generation from p-benzoquinone/UV: combined experimental and theoretical study. Appl. Catal., B 212, 150–158. https://doi.org/10.1016/j.apcatb.2017.03.081.
Gu, Y., Dong, W., Luo, C., Liu, T., 2016. Efficient reductive decomposition of perfluorooctanesulfonate in a high photon flux UV/Sulfite system. Environ. Sci. Technol. 50, 10554–10561. https://doi.org/10.1021/acs.est.6b03261.
Guo, M., Zhang, M., Liu, R., Zhang, X., Li, G., 2022. State-of-the-Art advancements in photocatalytic hydrogenation: reaction mechanism and recent progress in metal-organic framework (MOF)-based catalysts. Adv. Sci. 9, 2103361. https://doi.org/10.1002/advs.202103361.
Guo, Y., Li, Y., Shi, W., Yuan, J., Wang, L., Wang, Z., 2024. In situ redox growth of Pd/CuOx for enhanced electrocatalytic degradation of organic chlorides via indirect atomic H* reduction. Appl. Catal. B Environ. Energy 356, 124252. https://doi.org/10.1016/J.APCATB.2024.124252.
Guo, Y., Li, Y., Wang, Z., 2023. Electrocatalytic hydro-dehalogenation of halogenated organic pollutants from wastewater: a critical review. Water Res. 234, 119810. https://doi.org/10.1016/J.WATRES.2023.119810.
Han, L., Li, Q., Chen, S., Xie, W., Bao, W., Chang, L., Wang, J., 2017. A magnetically recoverable Fe3O4–NH2–Pd sorbent for capture of mercury from coal derived fuel gas. Sci. Rep. 7, 7448. https://doi.org/10.1038/s41598-017-07802-8.
Haque, M.M., Muneer, Mohd, Bahnemann, D.W., 2006. Semiconductor-mediated photocatalyzed degradation of a herbicide derivative, chlorotoluron, in aqueous suspensions. Environ. Sci. Technol. 40, 4765–4770. https://doi.org/10.1021/es060051h.
He, J., Boersma, M., Song, Z., Krebsbach, S., Fan, D., Duin, E.C., Wang, D., 2024. Biochar and surfactant synergistically enhanced PFAS destruction in UV/sulfite system at neutral pH. Chemosphere 353, 141562. https://doi.org/10.1016/J.CHEMOSPHERE.2024.141562.
Heiden, Z.M., Rauchfuss, T.B., 2007. Homogeneous catalytic reduction of dioxygen using transfer hydrogenation catalysts. J. Am. Chem. Soc. 129, 14303–14310. https://doi.org/10.1021/ja073774p.
Hernandez, J.E., Tanaka, N., Yamada, R., Wang, Y., Nishihara, K., Johzaki, T., Sunahara, A., Kang, K.S., Ueyama, S., Ozawa, K., Fujioka, S., 2024. Efficient photo-dissociation-induced production of hydrogen radicals using vacuum ultraviolet light from a laser-produced plasma. Appl. Phys. Lett. 124, 012101. https://doi.org/10.1063/5.0186829.
Hoke, J.B., Gramiccioni, G.A., Balko, E.N., 1992. Catalytic hydrodechlorination of chlorophenols. Appl. Catal., B 1, 285–296. https://doi.org/10.1016/0926-3373(92)80054-4.
Hu, W., Li, G.-X., Chen, J.-J., Huang, F.-J., Wu, Y., Yuan, S.-D., Zhong, L., Chen, Y.-Q., 2017. Enhanced catalytic performance of a PdO catalyst prepared via a two-step method of in situ reduction–oxidation. Chem. Commun. 53, 6160–6163. https://doi.org/10.1039/C7CC01997A.
Hurley, K.D., Shapley, J.R., 2007. Efficient heterogeneous catalytic reduction of perchlorate in water. Environ. Sci. Technol. 41, 2044–2049. https://doi.org/10.1021/es0624218.
Ioannidou, E., Ioannidi, A., Frontistis, Z., Antonopoulou, M., Tselios, C., Tsikritzis, D., Konstantinou, I., Kennou, S., Kondarides, D.I., Mantzavinos, D., 2016. Correlating the properties of hydrogenated titania to reaction kinetics and mechanism for the photocatalytic degradation of bisphenol A under solar irradiation. Appl. Catal., B 188, 65–76. https://doi.org/10.1016/J.APCATB.2016.01.060.
Jiang, W., Joens, J.A., Dionysiou, D.D., O'Shea, K.E., 2013. Optimization of photocatalytic performance of TiO2 coated glass microspheres using response surface methodology and the application for degradation of dimethyl phthalate. J. Photochem. Photobiol. Chem. 262, 7–13. https://doi.org/10.1016/J.JPHOTOCHEM.2013.04.008.
Jing, H., Sun, L., Xie, Q., Zhai, Y., Qi, C., Duan, B., Sun, X., Zhao, L., Zhang, M., Su, H., 2025. Preparation and catalytic performance study of Pd-Au bimetallic catalysts supported on polyaniline-derived nitrogen and phosphorus co-doped carbon for the selective hydrogenation of p-chloronitrobenzene. Appl. Catal. Gen. 702, 120332. https://doi.org/10.1016/j.apcata.2025.120332.
Karatok, M., Egle, T., Mehar, V., O'Connor, C.R., Yu, M.-H., Friend, C.M., Weaver, J.F., 2020. Reduction of oxidized Pd/Ag(111) surfaces by H2: sensitivity to PdO island size and dispersion. ACS Catal. 10, 10117–10124. https://doi.org/10.1021/acscatal.0c03037.
Keane, M.A., 2011. Supported transition metal catalysts for hydrodechlorination reactions. ChemCatChem 3, 800–821. https://doi.org/10.1002/cctc.201000432.
Köhler, K., Heidenreich, R.G., Krauter, J.G.E., Pietsch, J., 2002. Highly active palladium/activated carbon catalysts for heck reactions: correlation of activity, catalyst properties, and Pd leaching. Chem. Eur J. 8, 622–631. https://doi.org/10.1002/1521-3765(20020201)8:3<622::AID-CHEM622>3.0.CO;2-0.
Kibis, L.S., Stadnichenko, A.I., V Koscheev, S., Zaikovskii, V.I., Boronin, A.I., 2012. Highly oxidized palladium nanoparticles comprising Pd4+ species: spectroscopic and structural aspects, thermal stability, and reactivity. J. Phys. Chem. C 116, 19342–19348. https://doi.org/10.1021/jp305166k.
Kim, J.D., Choi, M.Y., Choi, H.C., 2016. Catalyst activity of carbon nanotube supported Pd catalysts for the hydrogenation of nitroarenes. Mater. Chem. Phys. 173, 404–411. https://doi.org/10.1016/j.matchemphys.2016.02.030.
Koga, K., 2020. Electronic and catalytic effects of single-atom Pd additives on the hydrogen sensing properties of Co3O4 nanoparticle films. ACS Appl. Mater. Interfaces 12, 20806–20823. https://doi.org/10.1021/acsami.9b23290.

Lai, F., Tian, F.X., Xu, B., Ye, W.K., Gao, Y.Q., Chen, C., Xing, H.B., Wang, B., Xie, M.J., Hu, X.J., 2022. A comparative study on the degradation of phenylurea herbicides by UV/persulfate process: Kinetics, mechanisms, energy demand and toxicity evaluation associated with DBPs. Chem. Eng. J. 428, 132088. https://doi.org/10.1016/J.CEJ.2021.132088.

Lan, L., Du, F., Xia, C., 2016. The reaction mechanism for highly effective hydrodechlorination of p-chlorophenol over a Pd/CNTs catalyst. RSC Adv. 6, 109023–109029. https://doi.org/10.1039/C6RA21213A.

Li, A., Zhao, X., Hou, Y., Liu, H., Wu, L., Qu, J., 2012. The electrocatalytic dechlorination of chloroacetic acids at electrodeposited Pd/fe-Modified carbon paper electrode. Appl. Catal., B 111–112, 628–635. https://doi.org/10.1016/J.APCATB.2011.11.016.

Li, C., Luo, R., Zhu, T., Zhao, Y., Xu, K., Wu, M., Wang, S., Dong, Y., Yang, M., 2025. Tailoring the Pd-BaO interface for superior efficiency and durability in perhydro-N-propylcarbazole dehydrogenation. Appl. Catal. B Environ. Energy 371, 125197. https://doi.org/10.1016/J.APCATB.2025.125197.

Li, D., Zheng, T., Liu, Y., Hou, D., Yao, K.K., Zhang, W., Song, H., He, H., Shi, W., Wang, L., Ma, J., 2020. A novel electro-fenton process characterized by aeration from inside a graphite felt electrode with enhanced electrogeneration of H2O2 and cycle of Fe3+/Fe2+. J. Hazard. Mater. 396, 122591. https://doi.org/10.1016/J.JHAZMAT.2020.122591.

Li, R., Dörfler, U., Munch, J.C., Schroll, R., 2017. Enhanced degradation of isoproturon in an agricultural soil by a sphingomonas sp. strain and a microbial consortium. Chemosphere 168, 1169–1176. https://doi.org/10.1016/J.CHEMOSPHERE.2016.10.084.

Li, X., Liu, Y., Hemminger, J.C., Penner, R.M., 2015. Catalytically activated palladium@platinum nanowires for accelerated hydrogen gas detection. ACS Nano 9, 3215–3225. https://doi.org/10.1021/acsnano.5b00302.

Li, Z., Liu, Z., Li, B., Liu, Z., Li, D., Wang, H., Li, Q., 2016. Hollow hemisphere-shaped macroporous graphene/tungsten carbide/platinum nanocomposite as an efficient electrocatalyst for the oxygen reduction reaction. Electrochim. Acta 221, 31–40. https://doi.org/10.1016/J.ELECTACTA.2016.10.157.

Liao, P., Al-Ani, Y., Malik Ismael, Z., Wu, X., 2015. Insights into the role of humic acid on Pd-catalytic electro-fenton transformation of toluene in groundwater. Sci. Rep. 5, 9239. https://doi.org/10.1038/srep09239.

Lin, J., Hu, Y., Xiao, J., Huang, Y., Wang, M., Yang, H., Zou, J., Yuan, B., Ma, J., 2021. Enhanced diclofenac elimination in Fe(II)/peracetic acid process by promoting Fe(III)/Fe(II) cycle with ABTS as electron shuttle. Chem. Eng. J. 420, 129692. https://doi.org/10.1016/J.CEJ.2021.129692.

Liu, L., Qiao, L.Q., Liu, F., Sun, Q.Y., Zhao, Y.F., Wang, X.L., Li, N., Jiang, H.L., Chen, X.F., Wang, M.L., Wu, Y.N., Zhao, R.S., 2024. Facile synthesis of hydroxylated triazine-based magnetic microporous organic network for ultrahigh adsorption of phenylurea herbicides: an experimental and density-functional theory study. J. Hazard. Mater. 465, 133468. https://doi.org/10.1016/J.JHAZMAT.2024.133468.

Liu, P., Huang, Z., Gao, X., Hong, X., Zhu, J., Wang, G., Wu, Y., Zeng, J., Zheng, X., 2022b. Synergy between palladium single atoms and nanoparticles via hydrogen spillover for enhancing CO2 photoreduction to CH4. Adv. Mater. 34, 2200057. https://doi.org/10.1002/adma.202200057.

Liu, Z., Lan, H., Wang, Y., Zhang, J., Qin, J., Zhang, R., Dong, N., 2022a. Highly efficient degradation of bisphenol A with persulfate activated by vacuum-ultraviolet/ultraviolet light (VUV/UV): experiments and theoretical calculations. Chem. Eng. J. 429, 132485. https://doi.org/10.1016/J.CEJ.2021.132485.

Lopez, A., Mascolo, G., Ciannarella, R., Tiravanti, G., 2001. Formation of volatile halogenated by-products during chlorination of isoproturon aqueous solutions. Chemosphere 45, 269–274. https://doi.org/10.1016/S0045-6535(00)00567-1.

Lundstedt, T., Seifert, E., Abramo, L., Thelin, B., Nyström, Å., Pettersen, J., Bergman, R., 1998. Experimental design and optimization. Chemometr. Intell. Lab. Syst. 42, 3–40. https://doi.org/10.1016/S0169-7439(98)00065-3.

Lv, J., Wu, S., Tian, Z., Ye, Y., Liu, J., Liang, C., 2019. Construction of PdO–Pd interfaces assisted by laser irradiation for enhanced electrocatalytic N2 reduction reaction. J. Mater. Chem. A 7, 12627–12634. https://doi.org/10.1039/C9TA02045D.

Marlatt, V.L., Martyniuk, C.J., 2017. Biological responses to phenylurea herbicides in fish and amphibians: new directions for characterizing mechanisms of toxicity. Comp. Biochem. Physiol. C Toxicol. Pharmacol. 194, 9–21. https://doi.org/10.1016/J.CBPC.2017.01.002.

Mazhari, M.P., Hamadanian, M., Mehipour, M., Jabbari, V., 2018. Central composite design (CCD) optimized synthesis of Fe3O4@SiO2@AgCl/Ag/Ag2S as a novel magnetic nano-photocatalyst for catalytic degradation of organic pollutants. J. Environ. Chem. Eng. 6, 7284–7293. https://doi.org/10.1016/J.JECE.2018.11.024.

Meher, S., Rana, R.K., 2019. A rational design of a Pd-based catalyst with a metal–metal oxide interface influencing molecular oxygen in the aerobic oxidation of alcohols. Green Chem. 21, 2494–2503. https://doi.org/10.1039/C9GC00116F.

Moussavi, G., Rezaei, M., 2017. Exploring the advanced oxidation/reduction processes in the VUV photoreactor for dechlorination and mineralization of trichloroacetic acid: parametric experiments, degradation pathway and bioassessment. Chem. Eng. J. 328, 331–342. https://doi.org/10.1016/J.CEJ.2017.07.006.

Navon, R., Eldad, S., Mackenzie, K., Kopinke, F.-D., 2012. Protection of palladium catalysts for hydrodechlorination of chlorinated organic compounds in wastewaters. Appl. Catal., B 119–120, 241–247. https://doi.org/10.1016/j.apcatb.2012.03.002.

Page, S.E., Sander, M., Arnold, W.A., McNeill, K., 2012. Hydroxyl radical formation upon oxidation of reduced humic acids by oxygen in the dark. Environ. Sci. Technol. 46, 1590–1597. https://doi.org/10.1021/es203836f.

Park, H., Vecitis, C.D., Cheng, J., Choi, W., Mader, B.T., Hoffmann, M.R., 2009. Reductive defluorination of aqueous perfluorinated alkyl surfactants: effects of ionic headgroup and chain length. J. Phys. Chem. A 113, 690–696. https://doi.org/10.1021/jp807116q.

Phan, N.T.S., Van Der Sluys, M., Jones, C.W., 2006. On the nature of the active species in palladium catalyzed mizoroki–heck and suzuki–miyaura couplings – homogeneous or heterogeneous catalysis, A critical review. Adv. Synth. Catal. 348, 609–679. https://doi.org/10.1002/adsc.200505473.

Proto, A., Cucciniello, R., Genga, A., Capacchione, C., 2015. A study on the catalytic hydrogenation of aldehydes using mayenite as active support for palladium. Catal. Commun. 68, 41–45. https://doi.org/10.1016/J.CATCOM.2015.04.028.

Prüsse, U., Vorlop, K.D., 2001. Supported bimetallic palladium catalysts for water-phase nitrate reduction. J. Mol. Catal. Chem. 173, 313–328. https://doi.org/10.1016/S1381-1169(01)00156-X.

Pucci, R., Angilella, G.G.N., 2022. Density functional theory, chemical reactivity, and the Fukui functions. Found. Chem. 24, 59–71. https://doi.org/10.1007/s10698-022-09416-z.

Qerimi, D., Panici, G., Jain, A., Jacobson, D., Ruzic, D.N., 2020. Study of a linear surface wave plasma source for tin removal in an extreme ultraviolet source. J. Vac. Sci. Technol. B 38, 052601. https://doi.org/10.1116/6.0000200.

Raizada, P., Kumari, J., Shandilya, P., Dhiman, R., Pratap Singh, V., Singh, P., 2017. Magnetically retrievable Bi2WO6/Fe3O4 immobilized on graphene sand composite for investigation of photocatalytic mineralization of oxytetracycline and ampicillin. Process Saf. Environ. Prot. 106, 104–116. https://doi.org/10.1016/J.PSEP.2016.12.012.

Rayaroth, M.P., Boczkaj, G., Aubry, O., Aravind, U.K., Aravindakumar, C.T., 2023. Advanced oxidation processes for degradation of water pollutants—ambivalent impact of carbonate species: a review. Water 15. https://doi.org/10.3390/w15081615.

Reed, A.E., Weinstock, R.B., Weinhold, F., 1985. Natural population analysis. J. Chem. Phys. 83, 735–746. https://doi.org/10.1063/1.449486.

Rehman, A., van de Kruijs, R.W.E., van den Beld, W.T.E., Sturm, J.M., Ackermann, M., 2023. Chemical interaction of hydrogen radicals (H*) with transition metal nitrides. J. Phys. Chem. C 127, 17770–17780. https://doi.org/10.1021/acs.jpcc.3c04490.

Rosal, R., Rodríguez, A., Perdigón-Melón, J.A., Petre, A., García-Calvo, E., Gómez, M.J., Agüera, A., Fernández-Alba, A.R., 2010. Occurrence of emerging pollutants in urban wastewater and their removal through biological treatment followed by ozonation. Water Res. 44, 578–588. https://doi.org/10.1016/J.WATRES.2009.07.004.

Rossmeisl, J., Chan, K., Skúlason, E., Björketun, M.E., Tripkovic, V., 2016. On the pH dependence of electrochemical proton transfer barriers. Catal. Today 262, 36–40. https://doi.org/10.1016/J.CATTOD.2015.08.016.

Samejo, B.A., Rayaroth, M.P., Wang, C., Sun, X., Boczkaj, G., 2025. Hydrated electrons and other reductive species - properties, formation and applications in advanced reduction processes for degradation of emerging organic pollutants – a review. Water Resour. Ind., 100311 https://doi.org/10.1016/J.WRI.2025.100311.

Saputera, W.H., Mul, G., Hamdy, M.S., 2015. Ti3+-containing titania: synthesis tactics and photocatalytic performance. Catal. Today 246, 60–66. https://doi.org/10.1016/J.CATTOD.2014.07.049.

Shao, M., 2011. Palladium-based electrocatalysts for hydrogen oxidation and oxygen reduction reactions. J. Power Sources 196, 2433–2444. https://doi.org/10.1016/J.JPOWSOUR.2010.10.093.

sheng Wang, Y., Yang, F., hua Liu, Z., Yuan, L., Li, G., 2015. Electrocatalytic degradation of aspen lignin over Pb/PbO2 electrode in alkali solution. Catal. Commun. 67, 49–53. https://doi.org/10.1016/J.CATCOM.2015.03.033.

Soares, O.S.G.P., Órfão, J.J.M., Pereira, M.F.R., 2011. Nitrate reduction in water catalysed by Pd–Cu on different supports. Desalination 279, 367–374. https://doi.org/10.1016/J.DESAL.2011.06.037.

Song, W., Li, J., Wang, Z., Fu, C., Zhang, X., Feng, J., Xu, Z., Song, Q., 2020. Degradation of bisphenol A by persulfate coupled with dithionite: optimization using response surface methodology and pathway. Sci. Total Environ. 699, 134258. https://doi.org/10.1016/J.SCITOTENV.2019.134258.

Sun, C., Lou, Z., Liu, Y., Fu, R., Zhou, X., Zhang, Z., Baig, S.A., Xu, X., 2015. Influence of environmental factors on the electrocatalytic dechlorination of 2,4-dichlorophenoxyacetic acid on nTiN doped Pd/Ni foam electrode. Chem. Eng. J. 281, 183–191. https://doi.org/10.1016/J.CEJ.2015.06.113.

Sun, J., Fu, Y., He, G., Sun, X., Wang, X., 2014. Catalytic hydrogenation of nitrophenols and nitrotoluenes over a palladium/graphene nanocomposite. Catal. Sci. Technol. 4, 1742–1748. https://doi.org/10.1039/C4CY00048J.

Suyana, P., Kr, S., Nair, B.N., Karunakaran, V., Mohamed, A.P., Warrier, K.G.K., Hareesh, U.S., 2016. A facile one pot synthetic approach for C3N4–ZnS composite interfaces as heterojunctions for sunlight-induced multifunctional photocatalytic applications. RSC Adv. 6, 17800–17809. https://doi.org/10.1039/C5RA27427C.

Tchikuala, E., Mourão, P., Nabais, J., 2017. Valorisation of natural fibres from African baobab wastes by the production of activated carbons for adsorption of diuron. Procedia Eng. 200, 399–407. https://doi.org/10.1016/J.PROENG.2017.07.056.

Thind, P.S., Kumari, D., John, S., 2018. TiO2/H2O2 mediated UV photocatalysis of chlorpyrifos: optimization of process parameters using response surface methodology. J. Environ. Chem. Eng. 6, 3602–3609. https://doi.org/10.1016/J.JECE.2017.05.031.

Tian, Y., Wei, Z., Zhang, K., Peng, S., Zhang, X., Liu, W., Chu, K., 2017. Three-dimensional phosphorus-doped graphene as an efficient metal-free electrocatalyst for electrochemical sensing. Sens. Actuators, B Chem. 241, 584–591. https://doi.org/10.1016/J.SNB.2016.10.113.

Tixier, C., Bogaerts, P., Sancelme, M., Bonnemoy, F., Twagilimana, L., Cuer, A., Bohatier, J., Veschambre, H., 2000. Fungal biodegradation of a phenylurea herbicide, diuron : structure and toxicity of metabolites. Pest Manag. Sci. 56, 455–462. https://doi.org/10.1002/(SICI)1526-4998(200005)56:5<455::AID-PS152>3.0.CO;2-Z.

V Buxton, G., Greenstock, C.L., Helman, W.P., Ross, A.B., 1988. Critical review of rate constants for reactions of hydrated electrons, hydrogen atoms and hydroxyl radicals (·OH/·O− in aqueous solution. J. Phys. Chem. Ref. Data 17, 513–886. https://doi.org/10.1063/1.555805.

V Lowry, G., Reinhard, M., 2000. Pd-Catalyzed TCE dechlorination in groundwater: solute effects, biological control, and oxidative catalyst regeneration. Environ. Sci. Technol. 34, 3217–3223. https://doi.org/10.1021/es991416j.

Waddell, P.M., Tian, L., Scavuzzo, A.R., Venigalla, L., Scholes, G.D., Carrow, B.P., 2023. Visible light-induced palladium–carbon bond weakening in catalytically relevant T-shaped complexes. Chem. Sci. 14, 14217–14228. https://doi.org/10.1039/D3SC02588H.

Wang, Z., Liu, H., Chen, L., Chou, L., Wang, X., 2013. Green and facile synthesis of carbon nanotube supported Pd nanoparticle catalysts and their application in the hydrogenation of nitrobenzene. J. Mater. Res. 28, 1326–1333. https://doi.org/10.1557/jmr.2013.101.

Wang, Z., Wang, Z., Wang, G., Zhang, Q., Wang, Q., Wang, W., 2023. New insight into biodegradation mechanism of phenylurea herbicides by cytochrome P450 enzymes: successive N-demethylation mechanism. Environ. Int. 182, 108332. https://doi.org/10.1016/J.ENVINT.2023.108332.

Wei, W., Wei, Z., Liu, D., Zhu, Y., 2018. Enhanced visible-light photocatalysis via back-electron transfer from palladium quantum dots to perylene diimide. Appl. Catal., B 230, 49–57. https://doi.org/10.1016/j.apcatb.2018.02.032.

Weigend, F., Ahlrichs, R., 2005. Balanced basis sets of split valence, triple zeta valence and quadruple zeta valence quality for H to rn: design and assessment of accuracy. Phys. Chem. Chem. Phys. 7, 3297–3305. https://doi.org/10.1039/B508541A.

Wiebe, R., Gaddy, V.L., 1934. The solubility of hydrogen in water at 0, 50, 75 and 100° from 25 to 1000 atmospheres. J. Am. Chem. Soc. 56, 76–79. https://doi.org/10.1021/ja01316a022.

Wilde, M., Fukutani, K., Ludwig, W., Brandt, B., Fischer, J.-H., Schauermann, S., Freund, H.-J., 2008. Influence of carbon deposition on the hydrogen distribution in Pd nanoparticles and their reactivity in olefin hydrogenation. Angew. Chem. Int. Ed. 47, 9289–9293. https://doi.org/10.1002/anie.200801923.

Wu, L., Yan, X., Yang, L., Shen, S., Li, Y., Yang, S., He, L., Chen, Y., Yang, S., Zhang, Z., 2023. Simultaneous efficient degradation and dechlorination of chloramphenicol using UV/sulfite reduction: mechanisms and product toxicity. Chem. Eng. J. 452, 139161. https://doi.org/10.1016/J.CEJ.2022.139161.

Wu, S., Shen, L., Lin, Y., Yin, K., Yang, C., 2021. Sulfite-based advanced oxidation and reduction processes for water treatment. Chem. Eng. J. 414, 128872. https://doi.org/10.1016/J.CEJ.2021.128872.

Xiao, Q., Wang, T., Yu, S., Yi, P., Li, L., 2017. Influence of UV lamp, sulfur(IV) concentration, and pH on bromate degradation in UV/sulfite systems: mechanisms and applications. Water Res. 111, 288–296. https://doi.org/10.1016/J.WATRES.2017.01.018.

Xie, S., Li, Y., Wang, C., Bin Low, K., Ye, K., Kim, D., Zhang, X., Li, Y., Zhang, Y., Shi, F., Ma, L., Ehrlich, S.N., Liu, F., 2023. Silica modulated palladium catalyst with superior activity for the selective catalytic reduction of nitrogen oxides with hydrogen. Appl. Catal., B 327, 122437. https://doi.org/10.1016/J.APCATB.2023.122437.

Xing, W., Yin, M., Lv, Q., Hu, Y., Liu, C., Zhang, J., 2014. Oxygen solubility, diffusion coefficient, and solution viscosity, rotating electrode methods and oxygen reduction. Electrocatalysts 1–31. https://doi.org/10.1016/B978-0-444-63278-4.00001-X.

Xu, J., Cao, Z., Liu, X., Zhao, H., Xiao, X., Wu, J., Xu, X., Zhou, J.L., 2016. Preparation of functionalized Pd/Fe-Fe3O4@MWCNTs nanomaterials for aqueous 2,4-dichlorophenol removal: interactions, influence factors, and kinetics. J. Hazard. Mater. 317, 656–666. https://doi.org/10.1016/J.JHAZMAT.2016.04.063.

Xu, J., Tan, L., Baig, S.A., Wu, D., Lv, X., Xu, X., 2013a. Dechlorination of 2,4-dichlorophenol by nanoscale magnetic Pd/Fe particles: effects of pH, temperature, common dissolved ions and humic acid. Chem. Eng. J. 231, 26–35. https://doi.org/10.1016/J.CEJ.2013.07.018.

Xu, J., Tang, J., Baig, S.A., Lv, X., Xu, X., 2013b. Enhanced dechlorination of 2,4-dichlorophenol by Pd/FeFe3O4 nanocomposites. J. Hazard. Mater. 244–245, 628–636. https://doi.org/10.1016/J.JHAZMAT.2012.10.051.

Xu, W., Lv, C., Zou, Y., Ren, J., She, X., Zhu, Y.K., Zhang, Y., Chen, S., Yang, X., Zhan, T., Sun, J., Yang, D., 2019. Mechanistic insight into high-efficiency sodium storage based on N/O/P-functionalized ultrathin carbon nanosheet. J. Power Sources 442, 227184. https://doi.org/10.1016/J.JPOWSOUR.2019.227184.

Yin, Y.B., Guo, S., Heck, K.N., Clark, C.A., Conrad, C.L., Wong, M.S., 2018. Treating water by degrading oxyanions using metallic nanostructures. ACS Sustain. Chem. Eng. 6, 11160–11175. https://doi.org/10.1021/acssuschemeng.8b02070.

Yoon, S., Han, D.S., Liu, X., Batchelor, B., Abdel-Wahab, A., 2014. Degradation of 1,2-dichloroethane using advanced reduction processes. J. Environ. Chem. Eng. 2, 731–737. https://doi.org/10.1016/J.JECE.2013.11.013.

Yu, X., Gocze, Z., Cabooter, D., Dewil, R., 2021. Efficient reduction of carbamazepine using UV-activated sulfite: assessment of critical process parameters and elucidation of radicals involved. Chem. Eng. J. 404, 126403. https://doi.org/10.1016/J.CEJ.2020.126403.

Yuan, S., Chen, M., Mao, X., Alshawabkeh, A.N., 2013. Effects of reduced sulfur compounds on Pd-Catalytic hydrodechlorination of trichloroethylene in groundwater by cathodic H2 under electrochemically induced oxidizing conditions. Environ. Sci. Technol. 47, 10502–10509. https://doi.org/10.1021/es402169d.

Yuranova, T., Franch, C., Palomares, A.E., Garcia-Bordejé, E., Kiwi-Minsker, L., 2012. Structured fibrous carbon-based catalysts for continuous nitrate removal from natural water. Appl. Catal., B 123–124, 221–228. https://doi.org/10.1016/J.APCATB.2012.04.007.

Zhang, Q., Lü, J., Ma, L., Lu, C., Liu, W., Li, X., 2013. Study on deactivation by sulfur and regeneration of Pd/C catalyst in hydrogenation of N-(3-nitro-4-methoxyphenyl) acetamide. Chin. J. Chem. Eng. 21, 622–626. https://doi.org/10.1016/S1004-9541(13)60497-8.

Zhang, Y., Zhang, J., Liu, Z., Wu, Y., Lv, Y., Xie, Y., Wang, H., 2022. Alloying iron into palladium nanoparticles for an efficient catalyst in acetylene dicarbonylation. Nanomaterials 12. https://doi.org/10.3390/nano12213803.

Zhao, J., Jing, W., Tan, T., Liu, X., Kang, Y., Wang, W., 2020. Etching high-fe-content PtPdFe nanoparticles as efficient catalysts towards glycerol electrooxidation. New J. Chem. 44, 4604–4612. https://doi.org/10.1039/C9NJ06259A.

Zhao, P., Qie, H., Cui, X., Zhang, W., Pu, T., Bao, W., Li, X., Lin, A., Ren, M., 2025. The effect of interfering ions on the degradation of organic pollutants by two types of activated persulfates over Fe-based catalysts in water: a meta-analysis. Chem. Eng. J. 509, 161123. https://doi.org/10.1016/J.CEJ.2025.161123.

Zhao, X., Chang, Y., Chen, W.-J., Wu, Q., Pan, X., Chen, K., Weng, B., 2022. Recent progress in Pd-Based nanocatalysts for selective hydrogenation. ACS Omega 7, 17–31. https://doi.org/10.1021/acsomega.1c06244.

Zhao, Y., Liang, W., Li, Y., Lefferts, L., 2017. Effect of chlorine on performance of Pd catalysts prepared via colloidal immobilization. Catal. Today 297, 308–315. https://doi.org/10.1016/J.CATTOD.2017.01.028.

Zhou, J., Lou, Z., Xu, J., Zhou, X., Yang, K., Gao, X., Zhang, Y., Xu, X., 2019. Enhanced electrocatalytic dechlorination by dispersed and moveable activated carbon supported palladium catalyst. Chem. Eng. J. 358, 1176–1185. https://doi.org/10.1016/J.CEJ.2018.10.098.

Zhu, B.-Z., Kitrossky, N., Chevion, M., 2000. Evidence for production of hydroxyl radicals by pentachlorophenol metabolites and hydrogen peroxide: a metal-independent organic fenton reaction. Biochem. Biophys. Res. Commun. 270, 942–946. https://doi.org/10.1006/bbrc.2000.2539.